

BIS(BIPYRIDYL)SILICON(IV) DIOLS AS POTENTIAL DUAL HYDROGEN BOND
DONORS FOR CATALYSIS

by

Crystal Kenee Waters

A thesis submitted to the faculty of
The University of North Carolina at Charlotte
in partial fulfillment of the requirements
for the degree of Master of Science in
Chemistry.

Charlotte

2016

Approved by:

Dr. Thomas A. Schmedake

Dr. Bernadette T. Donovan-Merkert

Dr. Daniel Rabinovich

Dr. Irina Nesmelova

© 2016
Crystal Kenee Waters
ALL RIGHTS RESERVED

ABSTRACT

CRYSTAL KENEE WATERS Bis(bipyridyl)silicon(IV) diols as potential dual hydrogen bond donors for catalysis (Under the direction of DR. THOMAS A. SCHMEDAKE).

Hydrogen bond donors (HBDs) have been explored as potential catalysts for the 1,4-conjugate addition and Diels-Alder reactions. HBD catalysis, which relies on Brønsted acid catalytic sites, is being explored as an oxygen and moisture stable alternative to transition metal catalysis. While most of the HBD catalysis field is based on organic catalysts, a few groups have explored silicon diols as potential dual hydrogen bond (DHB) catalysts.

In this project, two analogs of $[\text{Si}(\text{bpy})_2(\text{OH})_2]^{2+}$ were synthesized using different substituted 2,2'-bipyridine ligands including: 4,4'-dimethyl-2,2'-bipyridine (Me_2bpy) and 4,4'-bis(*tert*-butyl)-2,2'-bipyridine (${}^t\text{Bu}_2\text{bpy}$). Multinuclear Nuclear Magnetic Resonance (NMR), Infrared (IR) spectroscopies, and Elemental Analysis (EA) were used to characterize the complexes. X-ray crystallography was used to study the two compounds in the solid state. NMR kinetic studies were completed to determine if the silicon diols exhibited catalytic ability. A 1,4-conjugate addition reaction of N-methylindole (NMI) to trans- β -nitrostyrene (BNS) was used as the test reaction. The data suggest that the hexacoordinate silicon diols act as HBDs and have catalytic activity.

$[\text{Si}({}^t\text{Bu}_2\text{bpy})_2(\text{OH})_2](\text{PF}_6)_2$ was found to have superior catalytic properties over other silicon diols. Solvent and ions in solution effect the catalytic ability. Enantiomeric enrichment of $[\text{Si}(\text{Me}_2\text{bpy})_2(\text{OH})_2]\text{I}_2$ was successful and chiral catalysis is a future direction for the synthesized silicon diols.

DEDICATION

Earning a Master of Science in Chemistry is by far my greatest accomplishment to date. None of this would be possible without the loving support and continued encouragement from my family and friends along the way. To my beloved mother, thank you for standing in my corner when the world seemed to turn away. Thank you for providing for me all of these years and promoting my success. You always make sure I am financially, emotionally, and spiritually thriving. Your advice and opinions throughout my life have always mattered to me and as I grow they become even more important. Words cannot express my gratitude. To my father, thank you for supporting me throughout my educational career and providing me with financial support over the years. Thank you for your continued love and sacrifice to make sure I could continue my education even when finances were threatened. To my grandmother, Babe, I am forever grateful for the amount of encouragement, wisdom, love, and financial support you have blessed me with throughout my educational endeavors. I know you are very proud of me and I will continue to make you proud as I continue my educational career. I can only hope I live to be as wise and dependable as you have been to me since birth. To all of my deceased grandparents, you have blessed me with wonderful parents that have taught me well and for that I thank you. To all my family, I appreciate all you have done for me over the years. To my supportive friends, thank you for giving me an academic break to socialize. Lastly, but above all, I thank and praise God for blessing me with such a wonderful opportunity and accomplishment.

ACKNOWLEDGEMENTS

This work would not have been possible without the continued support, encouragement, and mentorship of my graduate research advisor, Dr. Thomas A. Schmedake. Joining your group I had minimal research experience yet you provided me an opportunity to explore my interests, learn to think as a research chemist, and mature as an individual. I am forever grateful for how much you have catapulted me forward in my educational journey and served as a listening ear when challenges arose and chemistry was tough.

To my committee members: Dr. Daniel Rabinovich, thank you for promoting my advancement into PhD programs and advocating on my behalf. Dr. Bernadette T. Donovan-Merkert, thank you for writing my letters of recommendation and being a role model to me as a female in chemistry. Dr. Irina Nesmelova, I appreciate your unexpected questions because they have challenged and advanced my critical thinking skills.

I would also like to thank the Schmedake group members, specifically Dr. Derek Peloquin, Tina Maguylo, David Lee, and the undergraduate students that worked with me on this project, including: Thanh Huyhn, Tram Le, Khadiya Ross, and Eric Maestas. Special thanks to the crystallographers, Dr. Dan Jones and Nemah-Allah Saleh.

I am very appreciative of the University of North Carolina at Charlotte and all of the faculty and staff in the chemistry department that aided in me being a part of this community and succeeding. I am forever grateful for the financial support provided by the university, the chemistry department, and the Graduate School. None of this work could have been completed without a UNC Charlotte Faculty Research Grant.

TABLE OF CONTENTS

LIST OF TABLES	viii
LIST OF FIGURES	ix
LIST OF SCHEMES	xii
LIST OF ABBREVIATIONS AND SYMBOLS	xiii
CHAPTER 1: HYDROGEN BOND DONORS AND THEIR ROLE AS CATALYST	1
1.1 Hydrogen Bond Donor Catalysis	1
1.2 Silicon Diols as DHB Catalyst	7
CHAPTER 2: SYNTHESIS AND CHARACTERIZATION OF BIS(BIPYRIDYL)SILICON(IV) DIOLS	13
2.1 Synthesis and Characterization of the Silicon Diols	13
2.2 Purification of the Silicon Diols	16
2.3 Physical Properties of Silicon Diols	18
2.4 Chiral Resolution	20
CHAPTER 3: BIS(BIPYRIDYL)SILICON(IV) DIOLS AS DUAL HYDROGEN BOND CATALYST	24
3.1 Recognition of Functionalities for Catalytic Binding	24
3.2 Catalysis: 1,4-Conjugate Addition Reaction	26
3.3 Nuclear Magnetic Resonance Kinetic Experiments	29
3.4 Comparing a Hexacoordinate Silicon Diol to a Tetracoordinate Silicon Diol	41
CHAPTER 4: EXPERIMENTAL DETAILS	44
4.1 General Synthesis Procedures	44
4.2 NMR Kinetic Experiments	47

4.3 Chiral Chromatography	47
CHAPTER 5: CONCLUSIONS AND FUTURE DIRECTIONS	49
5.1 Conclusions	49
5.2 Future Directions	50
REFERENCES	55
APPENDIX A: NMR AND IR FIGURES FOR THE SYNTHESIZED SILICON DIOLS	60
APPENDIX B: X-RAY ANALYSIS OF $[\text{Si}(\text{}^t\text{Bu}_2\text{bpy})_2(\text{OH})_2](\text{PF}_6)_2$	66
APPENDIX C: X-RAY ANALYSIS OF $[\text{Si}(\text{}^t\text{Bu}_2\text{bpy})_2(\text{OH})_2]\text{I}_2$	70
APPENDIX D: KINETIC EXPERIMENTS EXTRANEIOUS DATA	75

LIST OF TABLES

TABLE 1: Crystal data and structure refinement	66
TABLE 2: Bond lengths	67
TABLE 3: Bond Angles	68
TABLE 4: Crystal data and structure refinement	70
TABLE 5: Bond Lengths	70
TABLE 6: Bond Angles	71
TABLE 7: Fractional atomic coordinates ($\times 10^4$) and equivalent isotropic displacement parameters ($\text{\AA}^2 \times 10^3$)	72
TABLE 8: Anisotropic Displacement Parameters ($\text{\AA}^2 \times 10^3$)	74

LIST OF FIGURES

FIGURE 1: Examples of DHB donors including (thio)ureas, guanidinium, amidinium, BINOL, and bisphenol	3
FIGURE 2: Survey of the DHB catalysts studied by the Kozlowski group	4
FIGURE 3: Replotted data obtained from Kozlowski's survey of HBD catalytic efficiency of the Friedel-Crafts and Diels-Alder reaction	5
FIGURE 4: Thiourea analogs that the Seidel group tested as enantioselective DHB catalysts	6
FIGURE 5: 2-aminopyridinium ion studied as an enantioselective DHB donor	6
FIGURE 6: Equilibrium between the carbonyl and diol and the silicon analog	7
FIGURE 7: Silanediol cooperatively hydrogen bonded to an anion (chloride ion)	9
FIGURE 8: Diphenylsilanediol self-associating through hydrogen bonding interactions	9
FIGURE 9: Potential binding sites of developed hexacoordinate silicon diols	11
FIGURE 10: BINOL-derived silicon diol that is used for enantioselective catalysis by the Mattson group	12
FIGURE 11: ^1H NMR of $[\text{Si}(\text{}^t\text{Bu}_2\text{bpy})_2(\text{OH})_2](\text{PF}_6)_2$ in CD_3CN using Jeol 300MHz NMR	8
FIGURE 12: $[\text{Si}(\text{Me}_2\text{bpy})_2(\text{OH})_2](\text{PF}_6)_2$ ^1H NMR of the alkyl region	16
FIGURE 13: ^1H NMR of $[\text{Si}(\text{}^t\text{Bu}_2\text{bpy})_2(\text{OH})_2](\text{PF}_6)_2$	17
FIGURE 14: X-ray crystal structure of $[\text{Si}(\text{}^t\text{Bu}_2\text{bpy})_2(\text{OH})_2](\text{PF}_6)_2$ showing evidence of self-association in the solid state	19
FIGURE 15: Spectropolarimetry data obtained for $[\text{Si}(\text{Me}_2\text{bpy})_2(\text{OH})_2]\text{I}_2$ fractions collected	21

FIGURE 16: Maximum enantiomeric purity of both enantiomers of $[\text{Si}(\text{Me}_2\text{bpy})_2(\text{OH})_2]\text{I}_2$ in waters	22
FIGURE 17: Activation of a carbonyl group for nucleophilic attack using urea as a DHB donor	24
FIGURE 18: Activation of trans- β -nitrostyrene for nucleophilic attack using urea as a DHB donor	25
FIGURE 19: Proposed intermediate for the test reaction and DHB activation of the nitro- group	26
FIGURE 20: ^1H NMR scans of product formation for $[\text{Si}(\text{}^t\text{Bu}_2\text{bpy})_2(\text{OH})_2](\text{PF}_6)_2$ catalyzed reaction at 5 mol % on 500 MHz NMR	28
FIGURE 21: Uncatalyzed rate constant for the test reaction in CD_2Cl_2 , CDCl_3 and CD_3CN	29
FIGURE 22: Rate constant determination for the test reaction in CD_3CN using $[\text{Si}(\text{}^t\text{Bu}_2\text{bpy})_2(\text{OH})_2](\text{PF}_6)_2$ at 5 mol % loading at 30 °C	31
FIGURE 23: Rate constant determination for the test reaction in CDCl_3 using $[\text{Si}(\text{}^t\text{Bu}_2\text{bpy})_2(\text{OH})_2](\text{PF}_6)_2$ at 5 and 10 mol % at 30 °C	32
FIGURE 24: Rate constant determination for the test reaction in CD_2Cl_2 at 5 and 10 mol % at 30 degree Celsius	33
FIGURE 25: Relationship of the rate constant and catalyst concentration in chloroform, acetonitrile, and dichloromethane	34
FIGURE 26: Possibilities of catalyst inhibition due to coordination of CD_3CN in binding site or prevention of dimerization	35
FIGURE 27: Comparison between the PF_6^- and I^- salt of $[\text{Si}(\text{}^t\text{Bu}_2\text{bpy})_2(\text{OH})_2]^{2+}$ in chloroform with 5 mol % catalyst loading	36
FIGURE 28: Crystal structure of $[\text{Si}(\text{Me}_2\text{bpy})_2(\text{OH})_2]\text{I}_2$ with a H-I bond Length of 2.66Å suggesting that hydrogen bonding is occurring	38
FIGURE 29: $[\text{Si}(\text{Me}_2\text{bpy})_2(\text{OH})_2](\text{PF}_6)_2$ rate constant determination at 5 and 10 mol % loading in DCM at 30 °C	39
FIGURE 30: Error analysis within different experiments of the 0 mol %	40

catalyst loading in DCM providing the averaged rate constant	
FIGURE 31: Diphenyldihydroxysilane at 0, 5, 8, and 20 mol % loadings in DCM at 30 °C	41
FIGURE 32: Comparison of $[\text{Si}(\text{}^t\text{Bu}_2\text{bpy})_2(\text{OH})_2](\text{PF}_6)_2$ and $\text{Si}(\text{ph})_2(\text{OH})_2$ at 5 mol % loading in DCM	42
FIGURE 33: Relative enhanced rate of the silicon diols tested at the corresponding loading percentages	43
FIGURE 34: Potential symmetric and bulky asymmetric ligands that can be used to expand hexacoordinate silicon diols	50
FIGURE 35: Two enantiomers of the 4,4' substituted 2,2'-bipyridine silicon diols	51
FIGURE 36: Spartan calculated space filling of 5,5'-bis(<i>tert</i> -butyl)-2,2'-bipyridinesilicon(IV) diol coordinated to a 2-cyclohexen-1-one through cooperative hydrogen bonding	53
FIGURE 37: Example of a known silicon triol ⁵³	54
FIGURE 38: Hexacoordinate silicon diols activating an electrophile and a nucleophile simultaneously promoting a chiral addition product	54
FIGURE 39: Infrared spectroscopy data for $[\text{Si}(\text{Me}_2\text{bpy})_2(\text{OH})_2](\text{PF}_6)_2$	60
FIGURE 40: ^1H NMR of $[\text{Si}(\text{Me}_2\text{bpy})_2(\text{OH})_2]\text{I}_2$	61
FIGURE 41: ^1H NMR of $[\text{Si}(\text{Me}_2\text{bpy})_2(\text{OH})_2](\text{PF}_6)_2$	62
FIGURE 42: IR spectroscopy data for $[\text{Si}(\text{}^t\text{Bu}_2\text{bpy})_2(\text{OH})_2](\text{PF}_6)_2$	63
FIGURE 43: ^{29}Si NMR (99MHz) of the $[\text{Si}(\text{}^t\text{Bu}_2\text{bpy})_2(\text{OH})_2](\text{PF}_6)_2$	64
FIGURE 44: ^{13}C NMR (125MHz) of the $[\text{Si}(\text{}^t\text{Bu}_2\text{bpy})_2(\text{OH})_2](\text{PF}_6)_2$ in DCM	65
FIGURE 45: Comparison of 0 mol % catalyst loading in glass versus plastic NMR tubes in chloroform at 30 degrees Celsius	75
FIGURE 46: Kinetic experiment data to ensure no side products are formed	75
FIGURE 47: Error analysis of the 0 mol % reaction	76

LIST OF SCHEMES

SCHEME 1: Route to synthesize the bis(bipyridyl)dihydroxysilicon(IV) iodide analogs	13
SCHEME 2: Test reaction for kinetic studies of the silicon diols	26

LIST OF SYMBOLS AND ABBREVIATIONS

acac	acetylacetonato
BINOL	1,1-bi-2-naphthol
BNS	trans- β -nitrostyrene
bpy	2,2'-bipyridine
CD	circular dichroism
DCM	dichloromethane
DHB	dual hydrogen bond
EA	elemental microanalysis
ESI-MS	electrospray ionization mass spectrometry
HBD	hydrogen bond donor
HPLC	high performance liquid chromatography
HT	high tension (units of voltage)
IR	infrared spectroscopy
Me ₂ bpy	4,4'-dimethyl-2,2'-bipyridine
mdeg	millidegrees
NMI	N-methylindole
NMR	nuclear magnetic resonance
nonyl	4,4'-dinonyl-2,2'-bipyridine
RSD	relative standard deviation
%T	percent transmittance

t Bu ₂ bpy	4,4'-bis(<i>tert</i> -butyl)-2,2'-bipyridine
THF	tetrahydrofuran
UV-Vis	UV-Visible spectroscopy

CHAPTER 1: HYDROGEN BOND DONORS AND THIS ROLE AS CATALYSTS

1.1 Hydrogen Bond Donor Catalysis

Hydrogen bonding is a relatively strong intermolecular force that occurs when a proton and a more electronegative atom interact. These types of interactions were observed as early as the 19th century. A proton is very small, highly reactive, and known as the oldest catalyst for organic synthesis. Over the past decade or so chemists have studied how proton donors act as catalysts.^{1,2,3,4,5,6,7,8} Due to their efficiency hydrogen bond donor (HBD) catalysis is still being researched.

1.1.1 Lewis Acids Versus Brønsted Acids in Catalysis

Lewis acids are electron pair acceptors and are often used mainly for carbon-carbon bond formations. They have been used in Friedel-Crafts^{9,10,11}, Diels-Alder^{12,13,14}, and many other reactions¹⁵. These catalysts have also been known to promote nucleophilic addition of a C=X bond where X can be O, NR, or CR₂.¹⁶ Lewis acids tend to have high catalytic turnover numbers. Turnover number is the number of times a catalyst can be used to convert reactants to products without becoming poisoned or lowering its catalytic ability. Lewis acids catalysts are highly tunable which is important when designing an effective catalyst. To optimize rate enhancements, steric, electronic environment, and stereoselectivity can be tuned by manipulated the counterion and the ligand framework. Enantioselective catalysis of nucleophile-electrophile reactions have been studied using electrophile activation by metal-centered chiral Lewis acids^{17,18}.

There are also disadvantages to using Lewis acid catalyzed reaction. They tend to be unstable in oxygen and moisture conditions and some are not environmentally friendly. Thinking of potential applications in the chemical and pharmaceutical industries, many metals are poisonous and moving away from them to something less harmful is advantageous.

Nature uses a recognition process that relies on hydrogen bonding and hydrophobic interactions. Many enzymes have been shown to exert their catalytic activities through hydrogen bonding.^{19,20,21,22} These metal-free organocatalysts have received attention because of the design benefits. Hydrogen bonding catalysts have shown to be advantageous because they are environmentally benign, normally stable in water and oxygen conditions, and are potentially recoverable and recyclable. These metal-free Brønsted acids can also be enantioselective. Enantioselective studies have been completed and enantiomeric enrichments of the product have been quantified^{23,24}. More information on chiral DHBs is provided in section 1.1.3. A few groups have found a way to merge metal-templated catalysts with HBDs.^{25,26} This is a prominent avenue of study because it combines the benefits of both types of acid catalysis.

1.1.2 Hydrogen Bond Donors

Hydrogen bond donor (HBD) catalysts can act as Brønsted acids to catalyze reactions. Not only can these HBD catalysts hydrogen bond using one site, but some are dual hydrogen bond (DHB) donors. Examples of DHBs are shown in Figure 1.

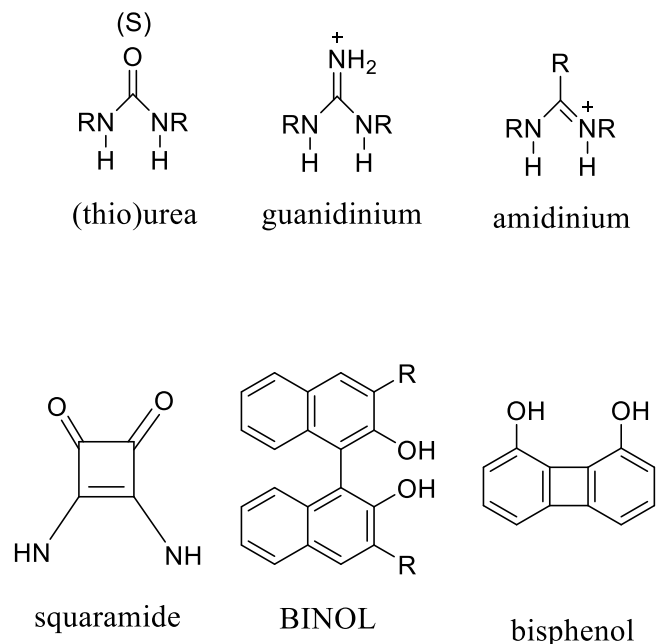


FIGURE 1: Examples of DHB donors including (thio)ureas, guanidinium, amidinium, squaramides, BINOL, and bisphenol

These organocatalysts possess two sites where hydrogen bonding can occur potentially enhancing the catalytic ability.

A quantitative assay of catalytic efficiency of a wide range of DHB donor catalyst was conducted by the Kozlowski group.²⁷ The catalysts, provided in Figure 2, were tested using a Diels-Alder and a Friedel-Crafts addition reaction. A graph of the catalytic rate enhancements for both reactions shows a strong correlation indicating that a catalyst that is efficient in catalyzing a Friedel-Crafts reaction is likely efficient at catalyzing a Diels-Alder reaction (Figure 3). This generality is attractive for developing a broadly useful catalyst. It also suggests that the Friedel-Crafts, or 1,4-conjugate addition, reaction is a good test reaction for developing efficient silicon diol catalysts. The graph also indicates a relationship between charge and catalytic efficiency for the DHB catalysts. The dicationic species catalyzed the reactions more efficiently than the monocationic and

the neutral species. This is not surprising considering the typical roles of HBD catalysts: anion coordination, stabilization of anionic transition states, and electrophilic activation.

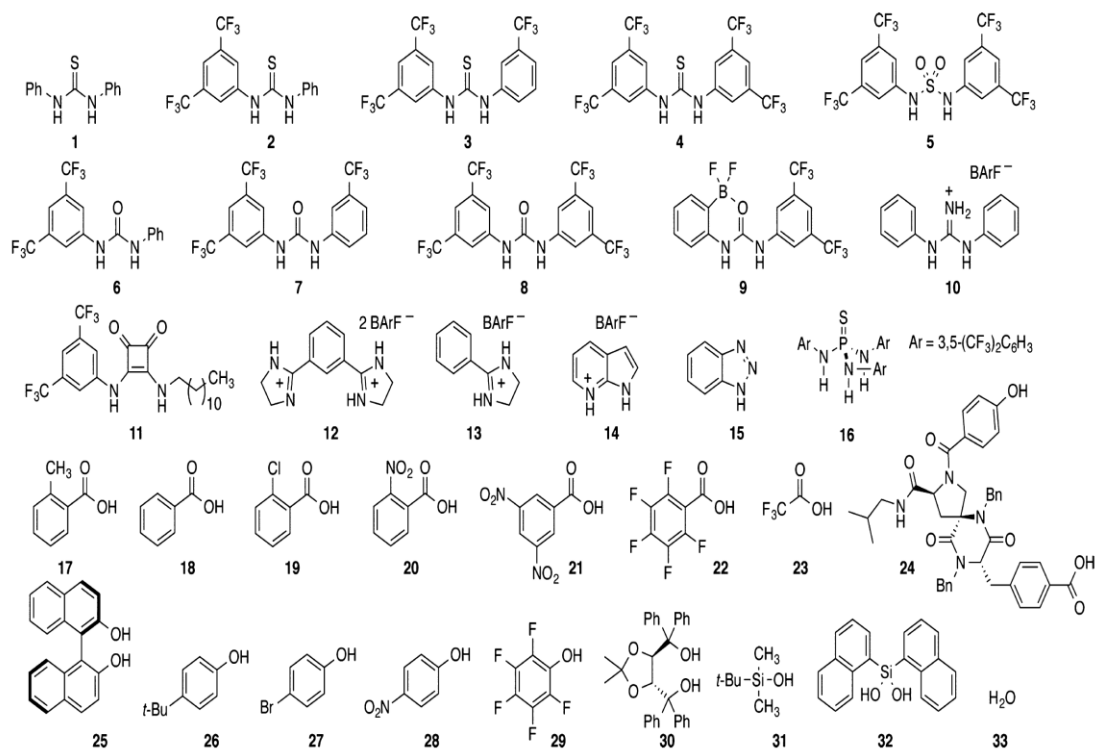


FIGURE 2: Survey of the HBD catalysts studied by the Kozłowski group²⁷

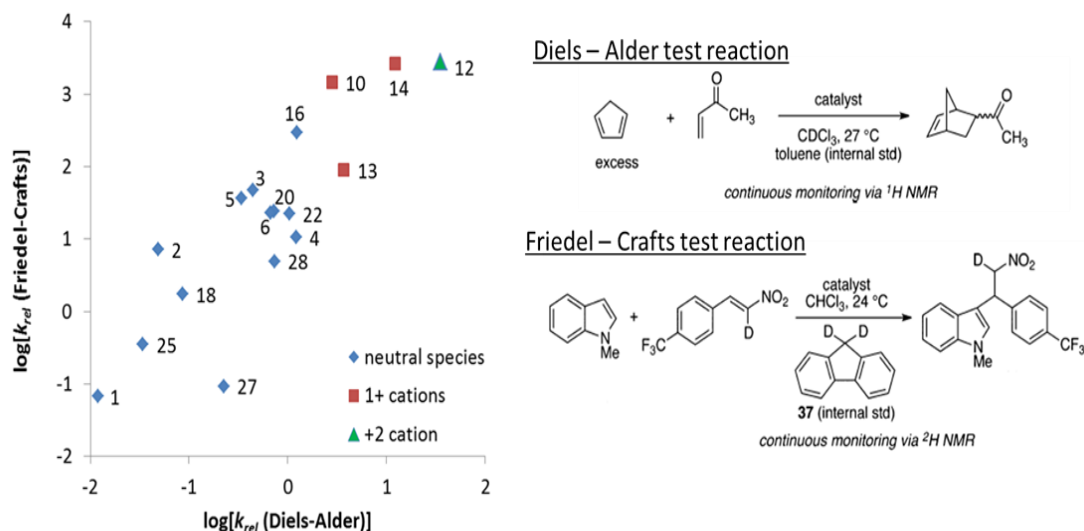


FIGURE 3: Replotted data obtained from Kozłowski's survey of HBD catalytic efficiency of the Friedel-Crafts and Diels-Alder reaction

When using HBD catalysts versus transition metals, there are some potential disadvantages. One of these deficiencies is that 5-10 mol % catalyst loading is required for catalytic efficiency.²⁸ The turnover numbers are typically lower than that of Lewis acids because of their inherent acidity. As previously mentioned, turnover number determines the robustness of the catalyst by quantifying the number of times the catalyst can convert reactants to products before becoming poisoned. The turnover frequency of HBDs also tends to be lower. Turnover frequency dictates how quickly the catalyst converts the reactants to products.

1.1.3 Chiral Hydrogen Bond Donors Used in Catalysis

Scientists have sought avenues to synthesize enantioselective dual hydrogen bond donors.²⁹ Analogs to ureas and thioureas have received a great deal of attention.³⁰ The Seidel group found that an analog to thiourea that has a charge associated with the species tended to catalyze the addition of indole to nitroalkenes (Figure 4).³¹

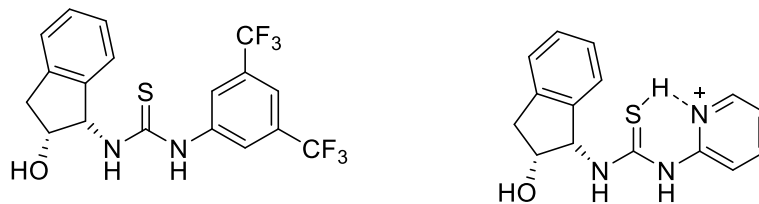


FIGURE 4: Thiourea analogs that the Seidel group tested as enantioselective DHB catalysts

The Seidel group determined that when an enantiopure catalyst is used, there is an enantiomeric enrichment in the product. When determining the effectiveness of the catalysts that were synthesized, many experimental parameters were manipulated such as the amount of catalyst that was loaded, as well as the solvent. To determine the enantiomeric enrichment, HPLC was used.

Another group also synthesized analogs to (thio)ureas and added an associated charge (Figure 5).³² The charge of these DHB donors tends to have a positive, linear correlation with the effectiveness of a catalyst. As the charge increases, the catalytic ability increases also. The 2-aminopyridinium ion was synthesized with ranging R-groups that were attached.

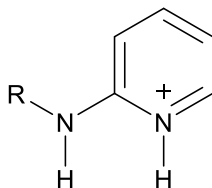


FIGURE 5: 2-aminopyridinium ion studied as an enantioselective DHB donor catalyst

Similarly to the Seidel group, the catalyst loading was changed to monitor the effects on the amount of product yielded as well as to determine the enantiomeric enrichment. By changing the R groups they were able to tune the enantioselectivity by changing the sterics and electronic environment. Using a bulky *tert*-butyl amide groups the group was able to yield the greatest enantiomeric enrichment in the product which was reported to be between 92-93%.

1.2 Silicon Diols as DHB Catalysts

While most of the HBD catalysis field has been based on organic catalysts, a few groups have started exploring silicon diols as potential DHB catalysts.³³ Although the chemistries of carbon and its heavier congener silicon are quite similar, one noticeable difference is the stability of the geminal silicon diol, as shown in Figure 6. In carbon analogs, the geminal diol quickly eliminates water to form the carbonyl compound, but the corresponding reaction does not occur with silicon diols. This provides a unique binding motif for the silicon diols in DHB catalysis.

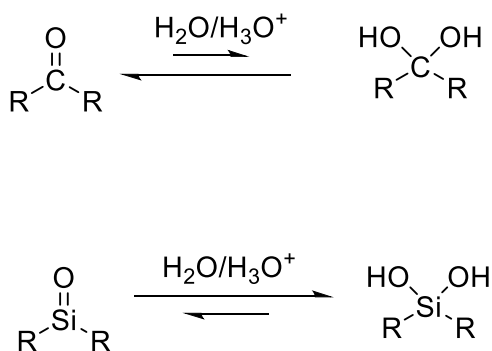


FIGURE 6: Equilibrium between the carbonyl and diol and the silicon analog

1.2.1 Silicon Diols as Dual Hydrogen Bond Donors

Silicon diols have become very interesting to study because of their unique ability to hydrogen bond. This is important for materials³⁴, surface chemistry, medicinal chemistry, and catalysis³⁵. Silanediols have been shown in a pharmaceutical application to be protease inhibitors and act as the active binding site of the metalloprotease.³⁶ These diols have also been used in surface chemistry, specifically chromatography. Silica gel is commonly used in chromatography to form hydrogen bonds with various types of organic and inorganic substances for purposes of separation. Silica gel has also been shown as an effective catalyst for electron-deficient nitro-olefins. It was shown to be an efficient, environmentally benign method for the 1,4-conjugate addition reaction of pyrrole and indole.³⁷

Silicon diols have recently become attractive to scholars because of their ability for molecular recognition using the hydroxyl groups of the silanol. Anion binding using silicon diols has been explored by a few groups.^{38,39} The Kondo group explored di(1-naphthyl)-silanediol to see if it could be used as an anion receptor. Using electrospray ionization mass spectrometry (ESI-MS), it was shown that when an acetate or chloride anion was titrated into the silicon diol sample, there was a 1:1 complex of the compound to the anion.³⁹ The goal of this study was to determine what type of hydrogen bonding was occurring, complexation or proton transfer of a Brønsted acid-type equilibrium. Using x-ray crystallography it was confirmed that cooperative hydrogen bonds were formed to the anion and to the solvent, chloroform (Figure 7).

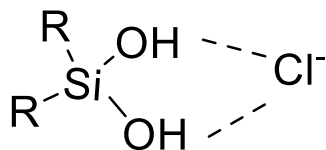


FIGURE 7: Silanediol cooperatively hydrogen bonded to an anion (chloride ion)

The ability for these silicon diols to cooperatively hydrogen bond to anions can be favorable for some applications, but for catalysis can yield unfavorable results such as catalyst inhibition. This catalytic inhibition is caused by anions in the site where electrophilic activation occurs.

DHB catalysts have the ability to self-recognize and form dimers. Sometimes these dimers form a more acidic proton, decreasing the pKa therefore enhancing the catalytic ability of these dual hydrogen bond catalysts.⁴⁰ An example of this self-association phenomenon is illustrated in Figure 8.

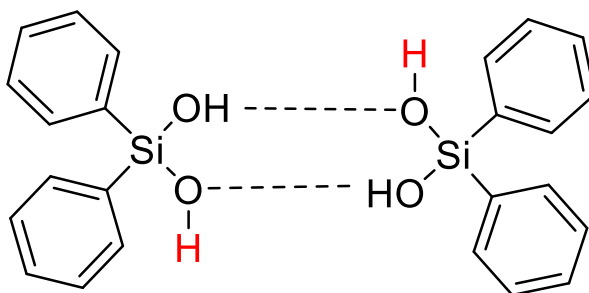


FIGURE 8: Diphenylsilanediol self-associating through hydrogen bonding interactions

The neutral DHB diphenylsilanediol, $\text{Ph}_2\text{Si}(\text{OH})_2$, shown in Figure 8 illustrates self-association that occurs. When compounds self-associate, they form more acidic hydrogens that are highlighted in red in the figure. Because of the decreased pKa, the catalytic efficiency of the silicon diol is enhanced.

Self-association is beneficial for catalysis, but may lower stereospecificity in chiral catalysis. To eliminate this phenomenon when developing bis(bipyridyl)silicon(IV) diols, it can be hypothesized that a charge associated with the compound will provide electrostatic repulsion, minimizing the ability of the compound to self-associate. The cation will need a non-coordinating counterion to ensure that anion binding does not poison or inhibit catalytic activity by blocking hydrogen bonding sites that can be used for electrophilic activation. Dual hydrogen bonding with a chiral C_2 symmetric ligand will result in a more defined binding site for the substrate than a single hydrogen bond interaction. This results in a prochiral substrate with potential attack at the *re* and *si* face. Using the proposed structure of the developed hexacoordinate silicon diols synthesized in this work, Figure 9 shows the different binding motifs to the substrate.

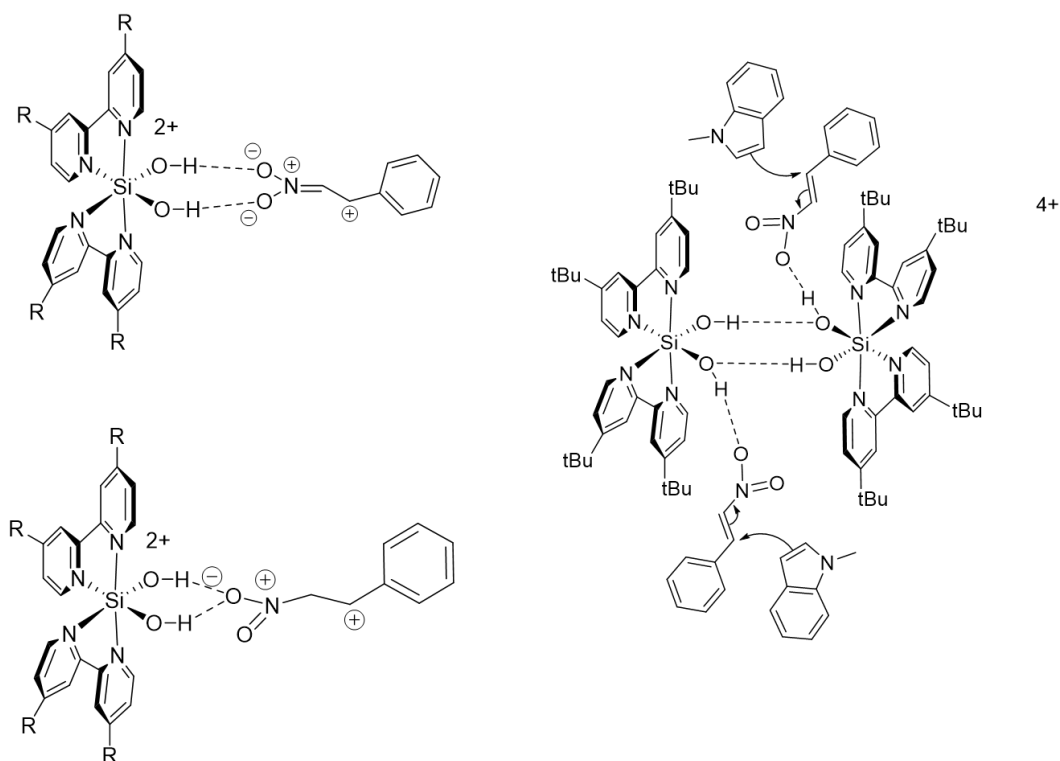


FIGURE 9: Potential binding sites of developed hexacoordinate silicon diols

1.2.2 Silicon Diols and their Chiral Properties

Silicon diols may have enhanced catalytic and enantioselectivity than other HBD catalysts. Few groups have studied chiral silicon diols.⁴¹ A BINOL-based silicon diol, shown in Figure 10, was investigated by Mattson's group as a potential chiral catalyst.⁴² These diols are able to be modified so they can be separated into their enantiopure forms. By controlling the anion-binding site, a silicon diol can be sterically hindered to preferentially yield an enantiomeric enrichment in the product.

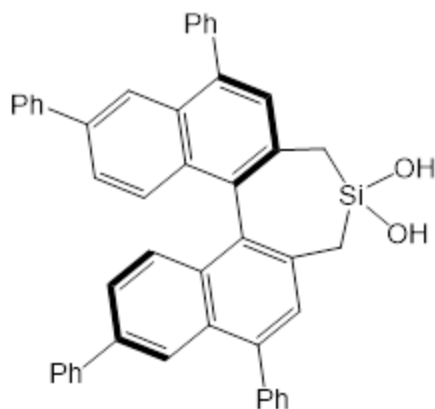


FIGURE 10: BINOL-derived silicon diol used for enantioselective catalysis by the Mattson group⁴²

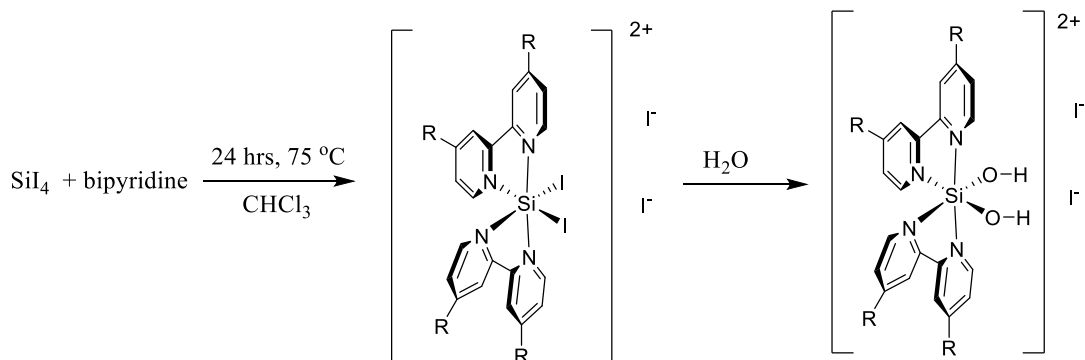
With the BINOL-derived silicon diol shown in the figure above, the phenyl rings were added to the structure because it added steric bulk which was found to increase the amount of enantiomeric enrichment. Using an enantiopure form of the silicon diol shown, there was roughly a 65% enantiomeric enrichment that was determined. It can be hypothesized that if this BINOL-based silicon diol provided enantiomeric enrichment in the product when an enantiopure catalyst was used, a more sterically hindered compound should be able to provide an enantiomeric enrichment and potentially have even greater enantioselectivity. Chiral properties of hexacoordinate silicon diols will be discussed further in Chapter 2.

CHAPTER 2: SYNTHESIS AND CHARACTERIZATION OF BIS(BIPYRIDYL)SILICON(IV) DIOLS

2.1 Synthesis of the Silicon Diols

Two analogs of bis(bipyridyl)dihydroxysilicon(IV) iodide have been synthesized. The archetypal complex, $[\text{Si}(\text{bpy})_2(\text{OH})_2]^{2+}$ was synthesized years ago.⁴³ Other bis(bipyridyl)silicon(IV) compounds have been synthesized by the Schmedake group to explore redox reactivity.⁴⁴ Catalytic efficiency has not been studied for these compounds thus far.

All syntheses were completed on a 0.500 gram or 1.00 gram scale. The ligands used were 4,4'-dimethyl-2,2'-bipyridine (Me_2bpy) or 4,4'-bis(*tert*-butyl)-2,2'-bipyridine (tBu_2bpy). The synthesis route is shown in Scheme 1. Detailed experimental information is provided in Chapter 4.



SCHEME 1: Synthesis route to bis(bipyridyl)dihydroxysilicon(IV) iodide analogs

To ensure no excess ligand remained after the synthesis of the Γ salt, ^1H NMR was used. The ^1H NMR of $[\text{Si}(\text{tBu}_2\text{bpy})_2(\text{OH})_2]\text{I}_2$ is shown in Figure 10. A more detailed labeling of the spectrum is provided in Appendix A.

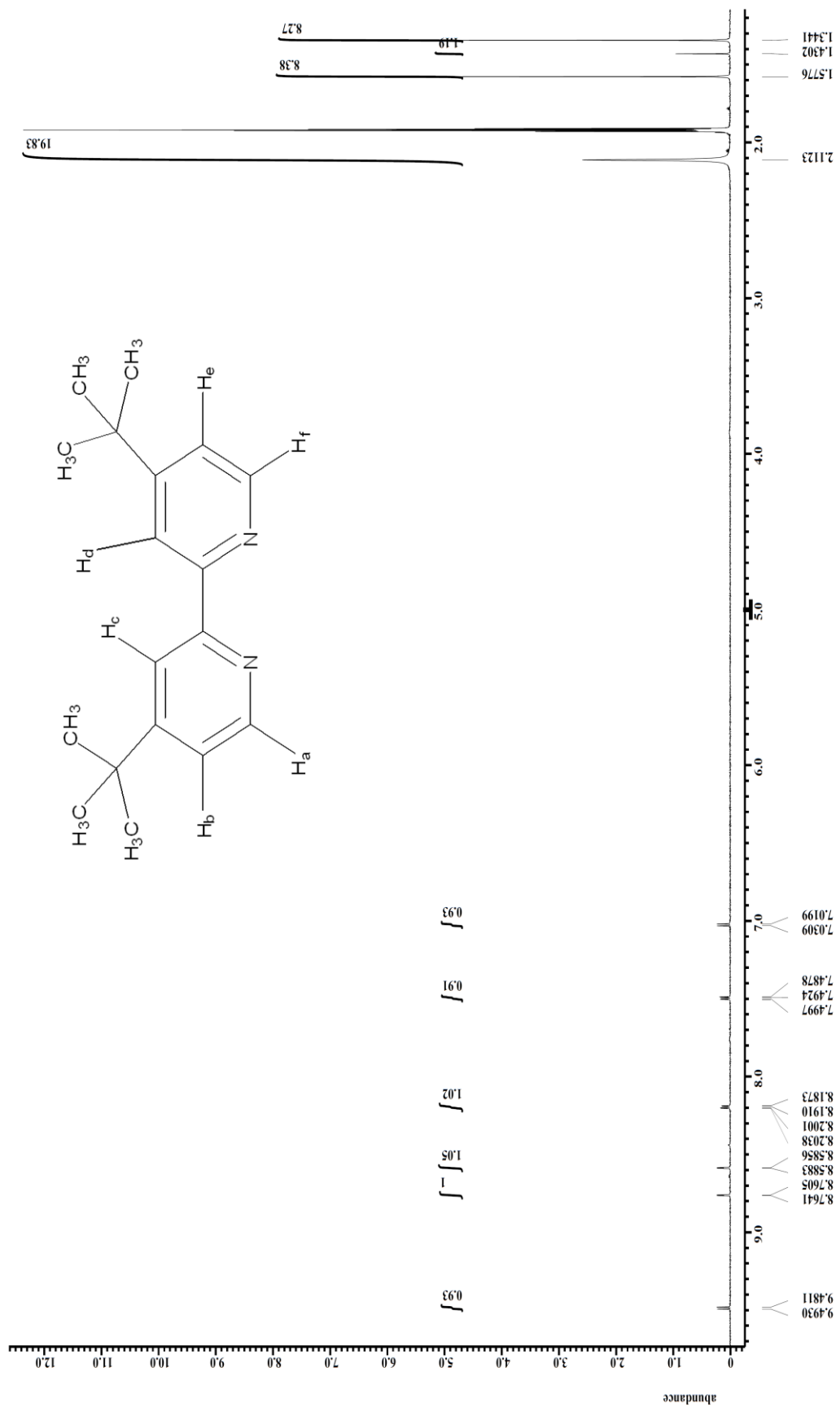


FIGURE 11: ^1H NMR of $[\text{Si}(\text{Bu}_2\text{bpy})_2(\text{OH})_2]_2$ in acetonitrile

2.2 Purification and Characterization of the Silicon Diols

Before catalysis can be tested, the compounds are converted to the PF_6^- salt. A metathesis reaction was completed and a dry solid was obtained.

$[\text{Si}(\text{Me}_2\text{bpy})_2(\text{OH})_2](\text{PF}_6)_2$ was characterized using ^1H NMR. The alkyl region of the compound is found in Figure 12. The full spectrum is provided Appendix A.

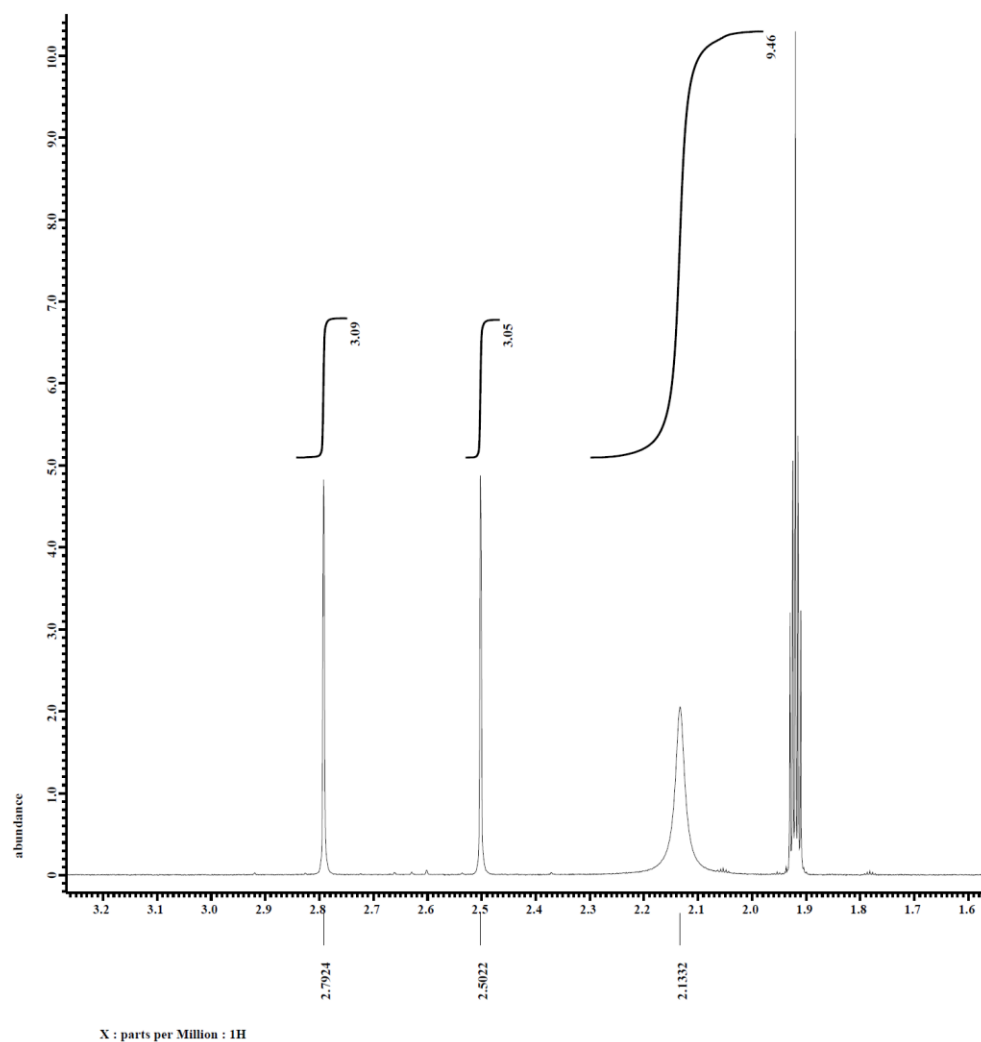
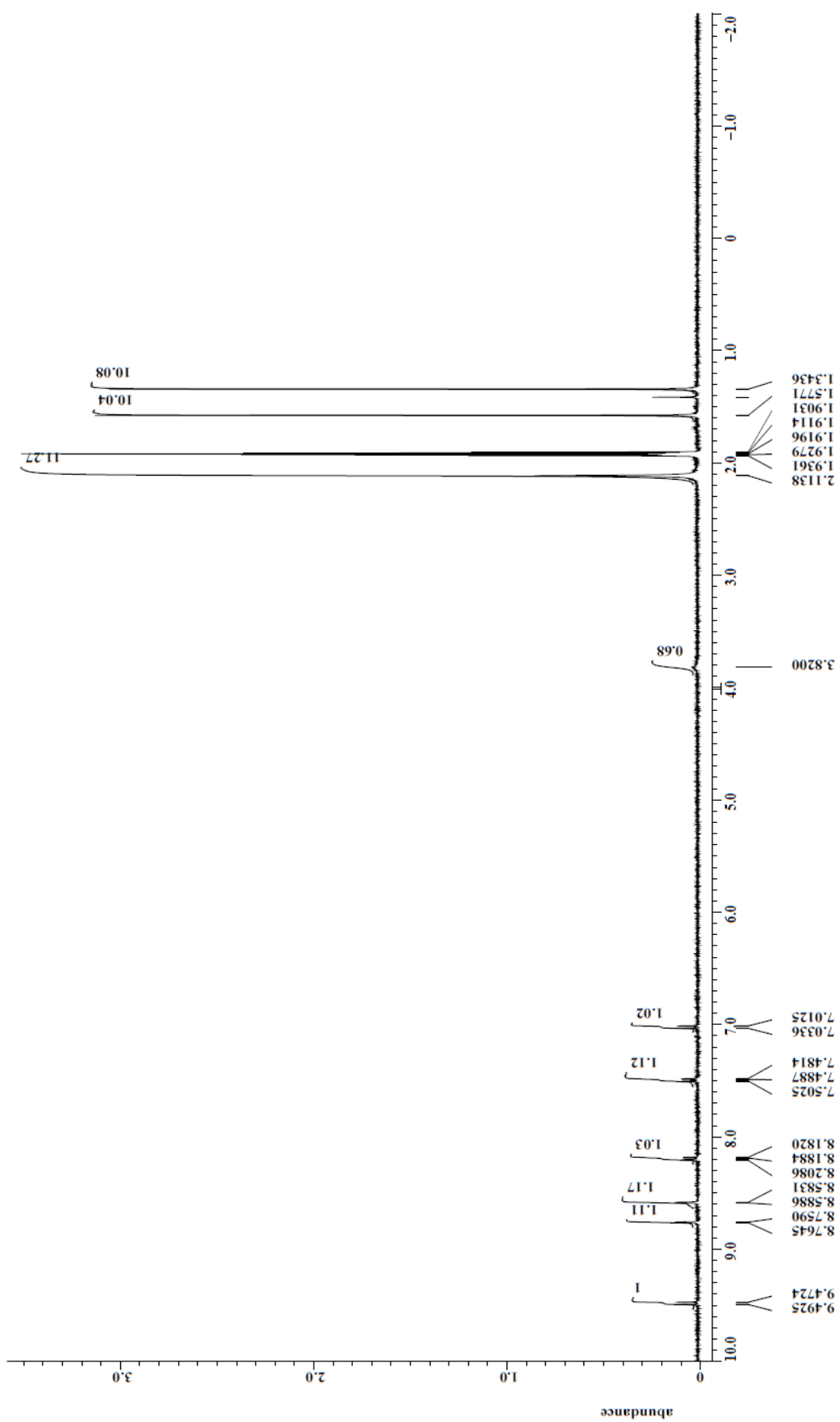


FIGURE 12: $[\text{Si}(\text{Me}_2\text{bpy})_2(\text{OH})_2](\text{PF}_6)_2$ ^1H NMR of the alkyl region

$[\text{Si}(\text{tBu}_2\text{bpy})_2(\text{OH})_2](\text{PF}_6)_2$ was also characterized using ^1H NMR (Figure 12).

FIGURE 13: ^1H NMR of $[\text{Si}(\text{Bu}_2\text{bpy})_2(\text{OH})_2](\text{PF}_6)_2$

Because the catalysis was completed using the PF_6^- salts, $[\text{Si}(\text{}^t\text{Bu}_2\text{bpy})_2(\text{OH})_2](\text{PF}_6)_2$ was also characterized using ^{29}Si and ^{13}C NMR, Infrared (IR) spectroscopy, X-ray crystallography, and elemental analysis (EA). All data is provided in Chapter 4. NMR and IR spectra are provided in Appendix A.

2.3 Physical Properties of the Silicon Diols

2.3.1 Solubility

The solubility of silicon diols changes with respect to the associated counterion as well as the alkyl substitution of the 2,2'-bipyridine ligands. Iodide salts are more soluble in aqueous solutions whereas hexafluorophosphate salts are more organic soluble.

Substituting the R- groups of the bipyridine ligand with increasingly long, branched chains affect how soluble the compound are in aqueous or organic solvents.

$[\text{Si}(\text{}^t\text{Bu}_2\text{bpy})_2(\text{OH})_2]\text{I}_2$ is more readily soluble in organic solvents than water because of the bulky *tert*-butyl groups attached to the bipyridine ligand. $[\text{Si}(\text{Me}_2\text{bpy})_2(\text{OH})_2]\text{I}_2$ is much more water soluble with more similar solubility characteristics to the unsubstituted bipyridine ligand.

Solubility is important to the application of catalysis. Because silicon diols have been shown to coordinate to anions, non-coordinating ions are necessary. With kinetic experiments, solubility is key. A catalyst must be fully soluble in the reaction solvent.

2.3.2 Aggregation and Self-Association: Solution and Solid State

Like other DHBs, silicon diols were shown to self-associate. These silicon diols were neutral and lacked electrostatic repulsion. For the dicationic hexacoordinate silicon diols developed, it was hypothesized that electrostatics would not allow self-association

to occur. With two hydrogens available for hydrogen bonding, the developed catalysts are expected to have higher enantioselectivity because there is a better chiral binding site.

Crystals of $[\text{Si}(\text{tBu}_2\text{bpy})_2(\text{OH})_2](\text{PF}_6)_2$ were grown using the vapor diffusion method. In the solid state, there is evidence of self-association which was not expected.

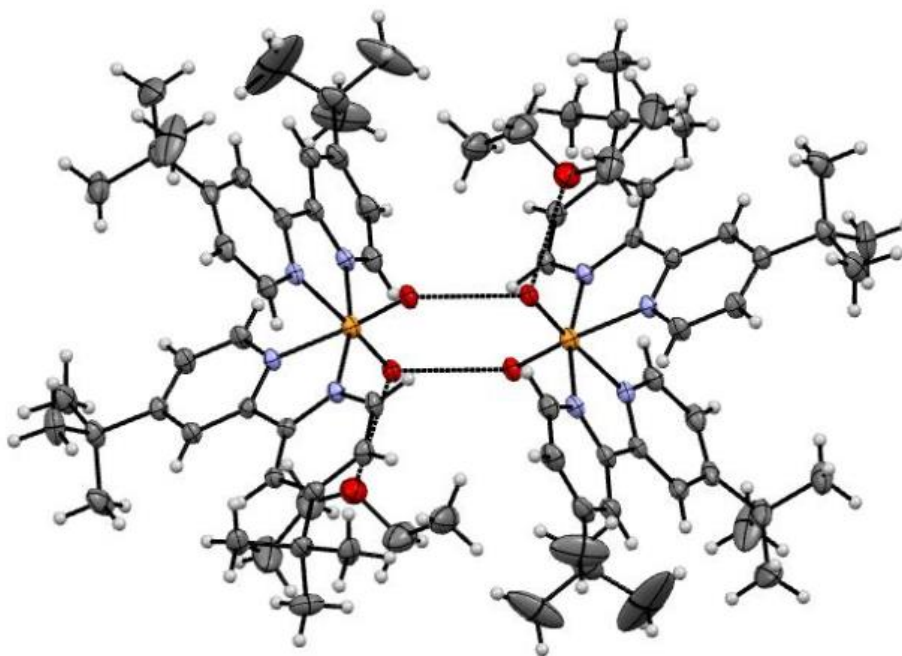


FIGURE 14: X-ray crystal structure of $[\text{Si}(\text{tBu}_2\text{bpy})_2(\text{OH})_2](\text{PF}_6)_2$ showing evidence of self-association in the solid state

Due to the disorder of the *tert*-butyl groups and the PF_6^- counterion, the hydrogens used in cooperative hydrogen bonding could not be located. It is expected that a hydrogen from one silicon diol is hydrogen bonding to the oxygen of the adjacent diol activating that hydrogen to have a lowered pKa. That activated hydrogen then hydrogen bonds to the solvent, diethyl ether. There were attempts at trying to eliminate hydrogen bonding to the solvent. The first attempt was to remove the crystals by storing them under vacuum

for 24 hours. The ether remain coordinated to the diols. The second was to use THF instead of diethyl ether as the diffusing solvent with the expectation that steric bulk would hinder solvent coordination.

The diffraction data does not allow for definitive placement of the hydrogen atoms of the diols; however, it can be deduced for the oxygen-oxygen bond distances that hydrogen bonding is occurring. The van der Waals radius of oxygen is 1.52 Å. Here, the O-O bond length between the diol and ether is 2.79 Å. Consequently, the O-O bond distances are shorter than the sum of their van der Waals radii, which is consistent with the hydrogen bonding taking place. All bond angles and bond lengths for the $[\text{Si}(\text{}^t\text{Bu}_2\text{bpy})_2(\text{OH})_2](\text{PF}_6)_2$ compound are provided in Appendix B.

2.4 Chiral Resolution

Hexacoordinate silicon diols have the ability to be enantiomerically resolved⁴⁵, purified, and subsequently used for chiral catalysis. The Yoshikawa group used a fractional crystallization method to resolve the enantiomers of the bis(bipyridyl)silicon(IV) diol using an enantiomerically pure tartrate salt. The group found that $[\text{Si}(\text{bpy})_2(\text{OH})_2]^{2+}$ racemized quickly in water. In this work, two methods were attempted to separate the enantiomers of the silicon diols: column chromatography and fractional crystallization. It was hypothesized that since the synthesized silicon diols were more organic soluble, they could be removed from water and racemization rates would decrease.

2.4.1 $[\text{Si}(\text{Me}_2\text{bpy})_2(\text{OH})_2]\text{I}_2$ Separations using Column Chromatography

To resolve the enantiomers of the $[\text{Si}(\text{Me}_2\text{bpy})_2(\text{OH})_2]\text{I}_2$ complex, column chromatography was completed. A 0.052 M (0.01289 mol/0.250 L) solution of

potassium antimonyl tartrate in water was used as the mobile phase. Exactly 10 mg of the $[\text{Si}(\text{Me}_2\text{bpy})_2(\text{OH})_2]\text{I}_2$ was dissolved in 2 mL of water to make a concentrated solution. Fractions of about 1 mL were collected. A band of colored material eluted from the column. Spectropolarimetry analysis was completed to see if there was an enantiomeric separation.

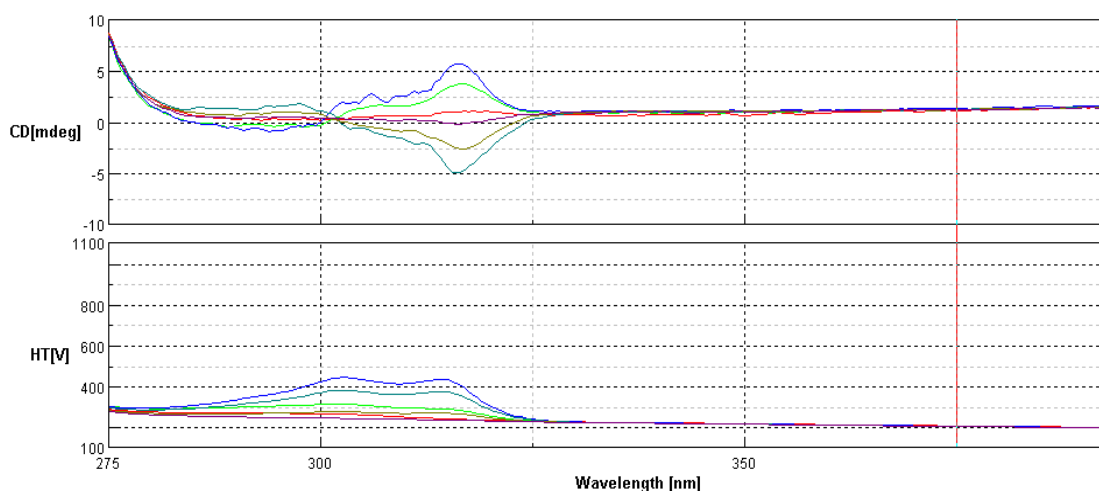


FIGURE 15: Spectropolarimetry data obtained for $[\text{Si}(\text{Me}_2\text{bpy})_2(\text{OH})_2]\text{I}_2$ fractions collected

Circular Dichroism (CD) allows for polarized light to shine on the compound. If the compound is chiral, it will rotate the light providing a signal of the rotation in millidegrees (mdeg). As shown in the spectropolarimetry data, as the fractions contained enriched material the rotation increased. Once one enantiomer eluted the column, roughly 1 mL later the other eluted. The figure above (Figure 15) provides an overlay of all of the fractions that contained enantiomeric enrichment. A more detailed look at the samples with greatest enantiomeric enrichment is provided in Figure 16.

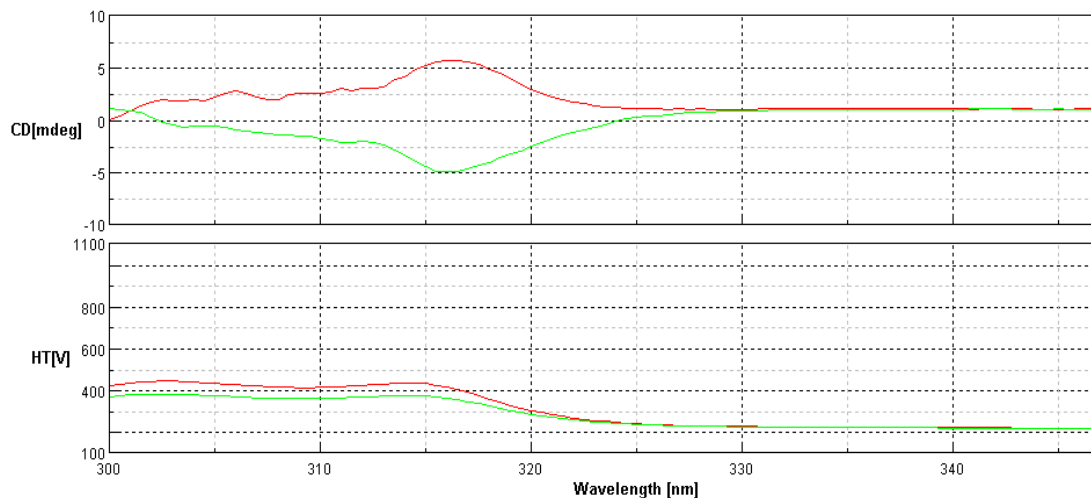


FIGURE 16: Maximum enantiomeric purity of both enantiomers of $[\text{Si}(\text{Me}_2\text{bpy})_2(\text{OH})_2]\text{I}_2$ in water

After running the material through the column, the counterion was switched from I^- to the corresponding tartrate salt. This adds an additional layer of purification that must be completed prior to doing catalytic experiments. For catalysis, a non-coordinating ion must be associated back with the enantiomerically pure cation. When attempting to convert the counterion to PF_6^- , ammonium hexafluorophosphate was added to the fractions that were enantiomerically enriched. Using a microcentrifuge a solid precipitate was obtained and allowed to dry overnight under vacuum. Once dry, the sample was dissolved in acetonitrile with the hopes that it would remain enantiomerically pure since it was not in water. UV-Vis was used to see if the compound remained in solution. Unfortunately, the precipitate was not the silicon diol as the PF_6^- salt, but rather excess NH_4PF_6 . Further purification techniques need to be explored to successfully exchange the counterion and retain enantiomeric purity of the catalyst. It is important to note that only qualitative results were obtained from the spectropolarimetry data. The exact

amount of enantiomeric purity was not quantified. Experimental details are provided in Chapter 4.

2.4.2 [Si(^tBu₂bpy)₂(OH)₂]₂I₂ enantiomeric resolution

Both methods, fractional crystallization and column chromatography was used with attempts to separate the enantiomers of the [Si(^tBu₂bpy)₂(OH)₂]₂I₂. A vapor diffusion method was used to grow crystals of the compound coordinated to the tartrate salt. Unfortunately, no crystals developed after seven days.

Column chromatography using a chiral mobile phase was used to separate the enantiomers. Experimental details can be found in Chapter 4. A flow cell was used to monitor when the enantiomers eluted the column. After spectropolarimetry analysis, it was determined that chiral chromatography was unsuccessful for the resolution of [Si(^tBu₂bpy)₂(OH)₂]₂I₂.

CHAPTER 3: BIS(BIPYRIDYL)SILICON(IV) DIOLS AS DUAL HYDROGEN BOND DONOR CATALYSTS

3.1 Recognition of Functionalities for Catalytic Binding

Dual hydrogen bond donors recognize particular functionalities such as nitro groups, anions, and oxyanion intermediates. Through this recognition, they stabilize carbocation and oxyanion intermediates and activate electrophiles for nucleophilic attack. Because of these functionalities they can catalyze reactions that have a reactant that can be activated through one of these groups. Silicon diols behave in a very similar manner.³⁵

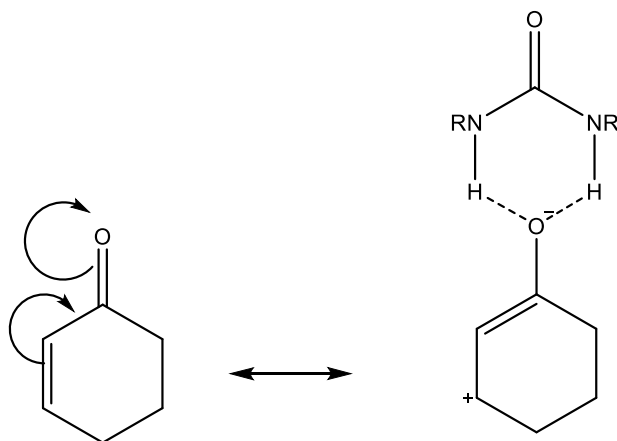


FIGURE 17: Activation of a carbonyl group for nucleophilic attack using urease as a DHB donor

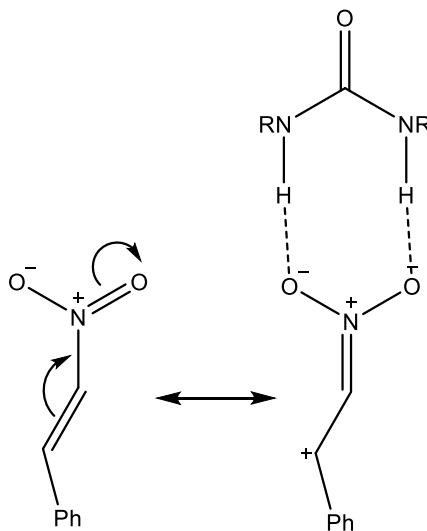


FIGURE 18: Activation of trans- β -nitrostyrene for nucleophilic attack using ureas as a DHB donor

Figures 17 and 18 show the activation of an electrophile through recognition of the two major functional groups, nitro and carbonyl groups. When testing catalytic ability of DHB donors, a common test reaction is used: a type of indole and a reaction with one of these recognizable functionalities (typically trans- β -nitrostyrene). Many researchers have tested HBD catalysts using this test reaction.^{46,47,48}

The work completed in this project uses the 1,4-conjugate addition reaction of N-methylindole (NMI) to trans- β -nitrostyrene (BNS). The synthesized hexacoordinate silicon diols will hydrogen bond to the nitro group of the BNS, activating the electrophile for nucleophilic attack by the NMI. Figure 19 is a proposed intermediate for the test reaction with electrophilic activation by the silicon diol.

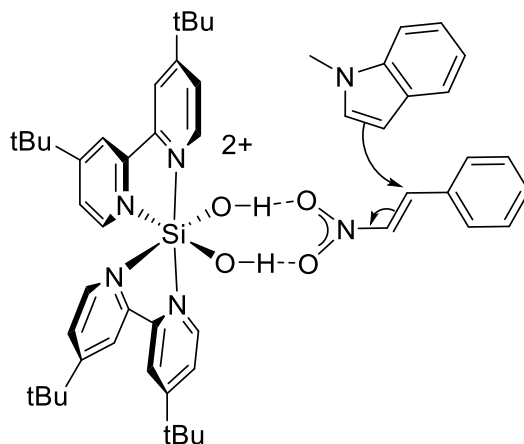
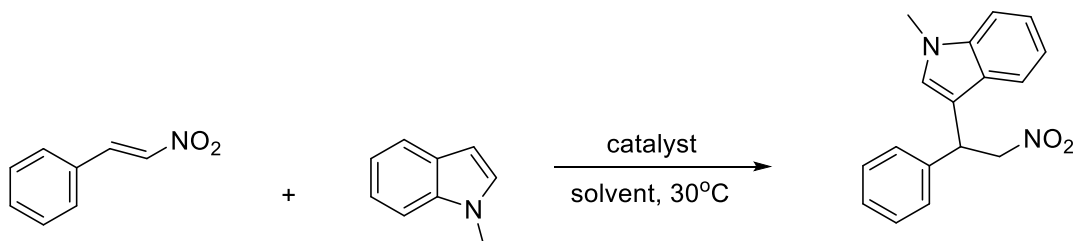


FIGURE 19: Proposed intermediate for the test reaction and DHB activation of the nitro-group

Several attempts to co-crystallize BNS with the silicon diol in a 1:1 mole ratio were unsuccessful. Using the vapor diffusion method and THF as the diffusing solvent, it was determined that the diol favors hydrogen bonding with the THF and the BNS was not coordinated to the silicon diol at all. THF was chosen as the diffusing solvent because it was previously determined that diethyl ether coordinates to the silicon diol.

3.2 Catalysis: 1,4-Conjugate Addition Reaction

The 1,4-conjugate addition reaction of NMI and BNS was used to demonstrate the effectiveness of the bis(bipyridyl)silicon(IV) diols (Scheme 2). A benefit to using this test reaction is that the synthesis is useful in many biologically relevant compounds.³⁰



SCHEME 2: Test reaction for kinetic studies of the synthesized silicon diols

The reaction was completed under pseudo-first order conditions with respect to NMI. BNS was in excess at 4 M (0.600 g), NMI at 0.4 M (50 μ L), and a corresponding mole percent of catalyst was added. The reason pseudo-first order conditions were completed with respect to NMI is so that the N-methyl shift can be monitored using ^1H NMR to quantify the amount of product that has been formed. Figure 19 shows that the N-methyl peak shifts from roughly 3.7 ppm (reactant) to 3.6 ppm (product). The intensities can be integrated to determine the rate constant. Experimental details for these kinetic experiments are provided in Chapter 4.

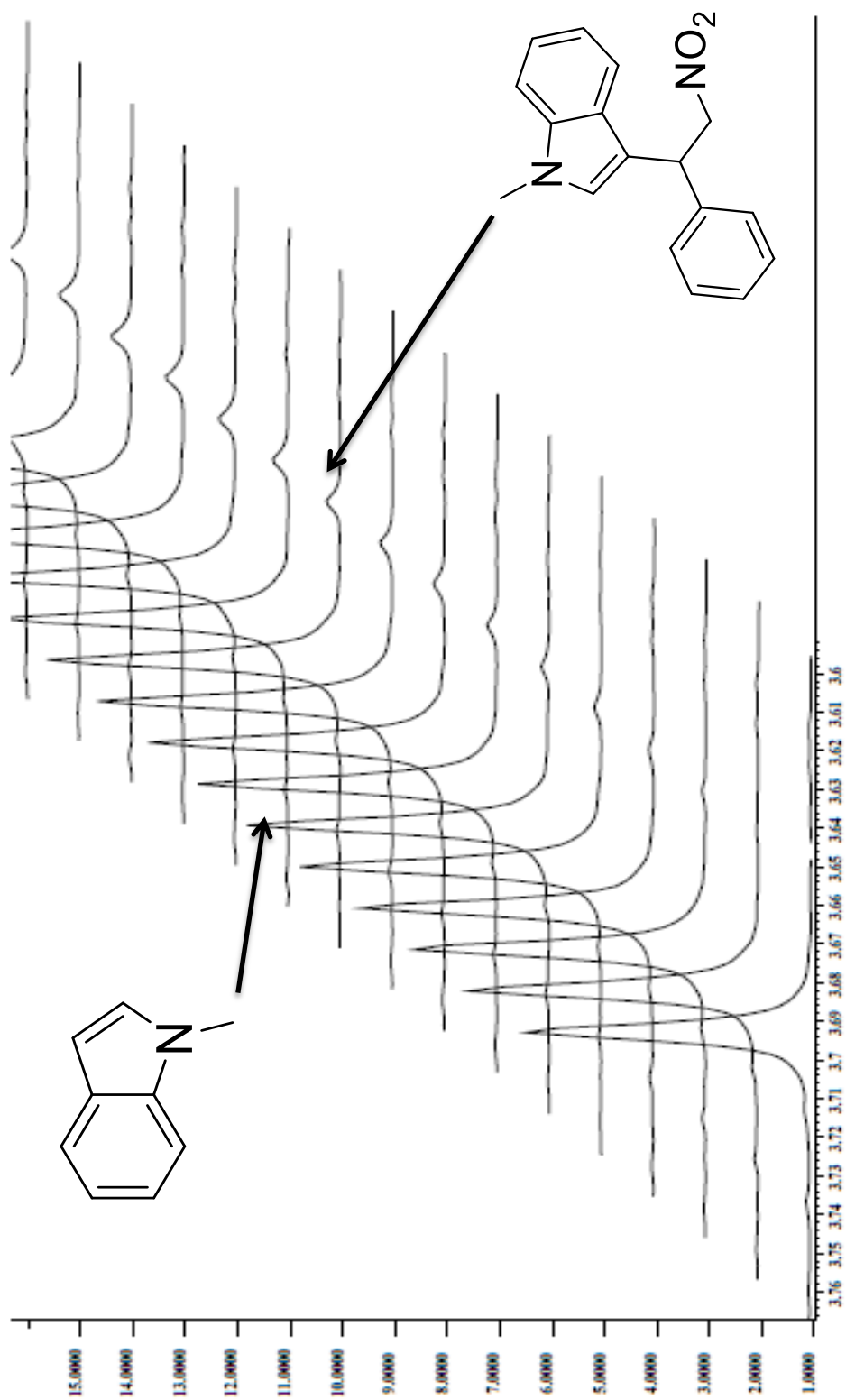


FIGURE 20: ^1H NMR scans of product formation for $[\text{Si}(\text{tBu}_2\text{bpy})_2(\text{OH})_2](\text{PF}_6)_2$ catalyzed reaction at 5 mol % on 500 MHz NMR

3.3 Nuclear Magnetic Resonance Kinetic Experiments

3.3.1 $[\text{Si}(\text{tBu}_2\text{bpy})_2(\text{OH})_2](\text{PF}_6)_2$ as a DHB catalyst

Kinetic experiments were performed under different experimental parameters was to optimize the conditions necessary to catalyze the 1,4-conjugate addition reaction. The first consideration was solvent effects. The uncatalyzed, or 0 mol % catalyst loading, was completed in 3 different solvents: chloroform, acetonitrile, and dichloromethane (Figure 21). The uncatalyzed rate constant was determined for each solvent. These rate constants were consequently used to calculate the rate enhancement after the addition of catalyst for each test reaction.

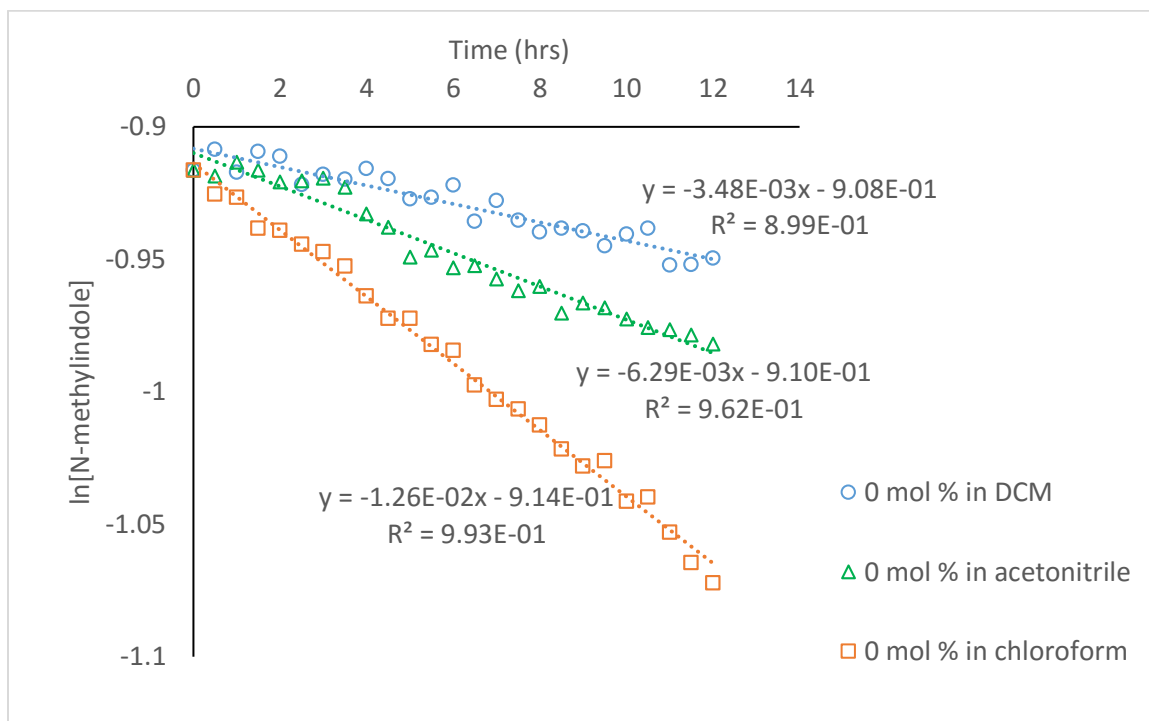


FIGURE 21: Uncatalyzed rate constant for the test reaction in CD_2Cl_2 , CDCl_3 , and CD_3CN

The slope of each linear regression represents the rate constant. The uncatalyzed rate was found to be the slowest in dichloromethane ($k = 3.48 \times 10^{-3} \text{ M}^{-1}\text{hr}^{-1}$), followed by acetonitrile ($k = 6.29 \times 10^{-3} \text{ M}^{-1}\text{hr}^{-1}$), and then in chloroform ($k = 1.26 \times 10^{-2} \text{ M}^{-1}\text{hr}^{-1}$).

The importance of considering this information is that the relative rate of enhancement accounts for the rate of the catalyzed and uncatalyzed reaction and is calculated as

$$k_{enhanced} = \frac{k_{cat} - k_{uncat}}{k_{uncat}}$$

This accounts for the enhancement of the catalyst on the reaction rate, as well as the part of the reaction that proceeds whether or not the catalyst is present. The larger the difference between the two, the greater the relative rate of enhancement.

After a baseline was established, a stoichiometric amount of $[\text{Si}(\text{}^t\text{Bu}_2\text{bpy})_2(\text{OH})_2](\text{PF}_6)_2$ was loaded into the reaction tube to determine catalytic enhancements. Figure 22 shows the experiment completed in acetonitrile using 0 and 5 mol % catalyst loading.

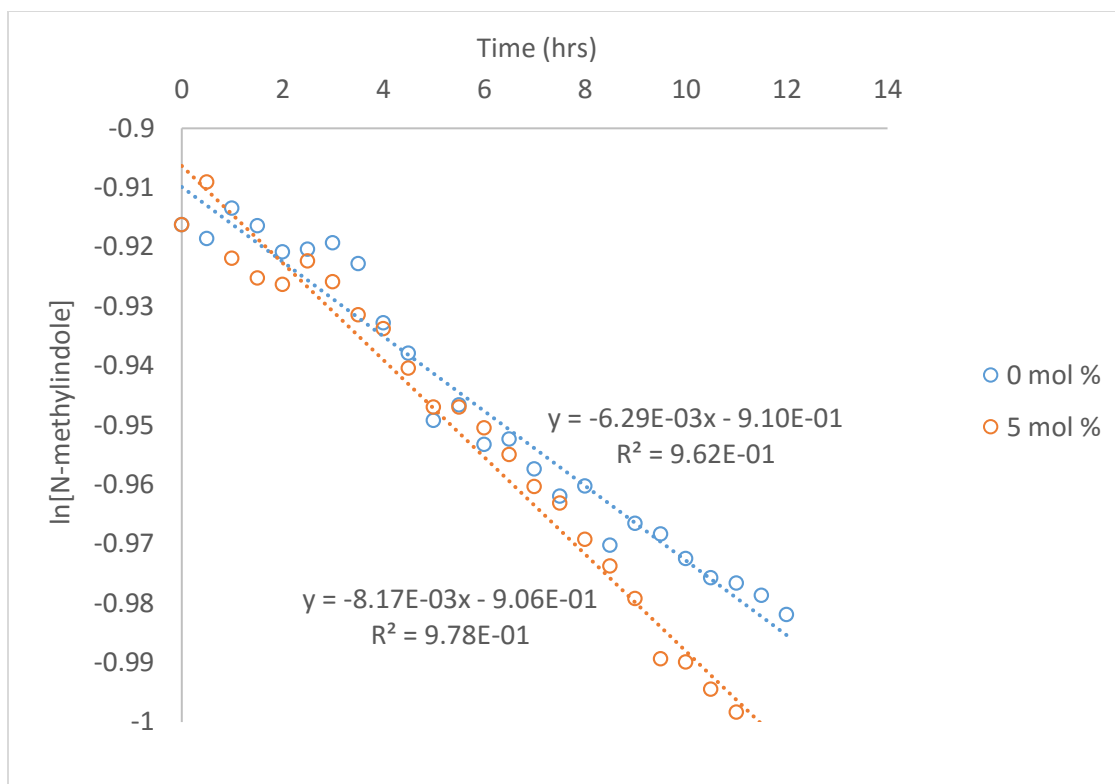


FIGURE 22: Rate constant determination for the test reaction in CD_3CN using $[Si(^tBu_2bpy)_2(OH)_2](PF_6)_2$ at 5 mol % loading at 30 °C

The uncatalyzed reaction has a $k = 6.29 \times 10^{-3} M^{-1}hr^{-1}$ whereas the 5 mol % catalyst loading has a $k = 8.17 \times 10^{-3} M^{-1}hr^{-1}$. The enhanced relative rate (k_{en}) has been found for this experiment to be 0.29. In acetonitrile, the catalyst is ineffective.

The exact same experiment was completed using chloroform (Figure 23).

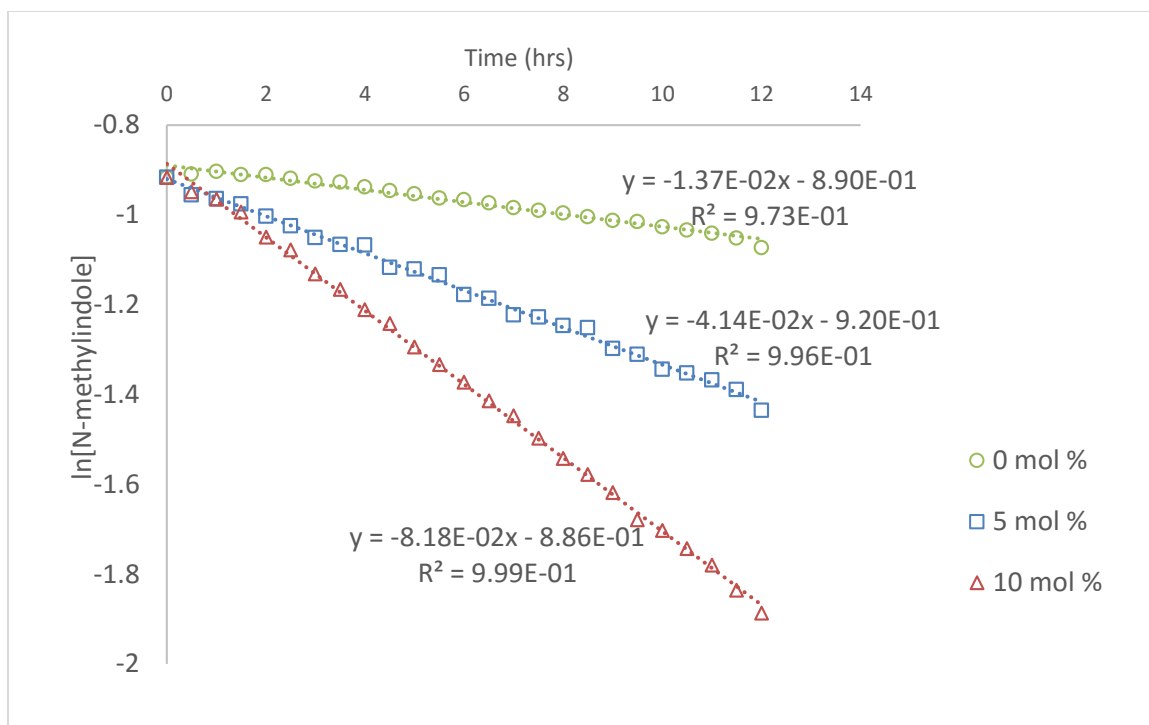


FIGURE 23: Rate constant determination for the test reaction in CDCl_3 using $[\text{Si}(\text{tBu}_2\text{bpy})_2(\text{OH})_2](\text{PF}_6)_2$ at 5 and 10 mol % at 30°C

At 0 mol %, the rate constant in chloroform is $1.37 \times 10^{-2} \text{ M}^{-1}\text{hr}^{-1}$, with a 5 mol % catalyst loading $k = 4.14 \times 10^{-2} \text{ M}^{-1}\text{hr}^{-1}$, and with a 10 mol % loading $k = 8.18 \times 10^{-2} \text{ M}^{-1}\text{hr}^{-1}$. This gives a k_{en} of 2.02 and 4.97 for the 5 and 10 mol % loading, respectively. Comparing CD_3CN to CDCl_3 , the latter provides greater catalytic enhancement and is therefore a better solvent for this test reaction.

The final experiment was completed with dichloromethane. The results are provided in Figure 24. The k_{en} for the 5 and 10 mol % catalyst loadings in CD_2Cl_2 were calculated to be 4.84 and 10.52, respectively.

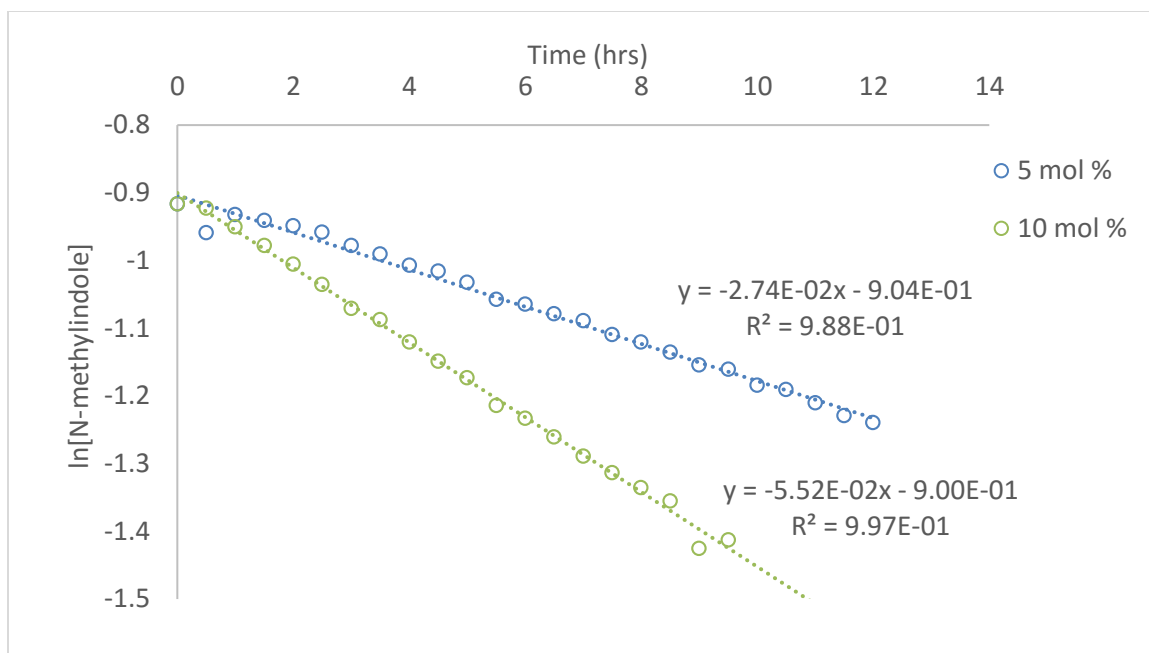


FIGURE 24: Rate law determination for the test reaction in CD_2Cl_2 using $[\text{Si}(\text{tBu}_2\text{bpy})_2(\text{OH})_2](\text{PF}_6)_2$ at 5 and 10 mol % loading at 30 °C

The catalyst has comparable effects in DCM and chloroform, but is not effective in acetonitrile (Figure 24). However, the solubility of the diols in chloroform are much lower, and the solubility limit of $[\text{Si}(\text{tBu}_2\text{bpy})_2(\text{OH})_2](\text{PF}_6)_2$ is around 10 mol %.

$[\text{Si}(\text{tBu}_2\text{bpy})_2(\text{OH})_2](\text{PF}_6)_2$ is the most soluble in dichloromethane. Figure 25 illustrates the results that were obtained in the three different solvents that were tested.

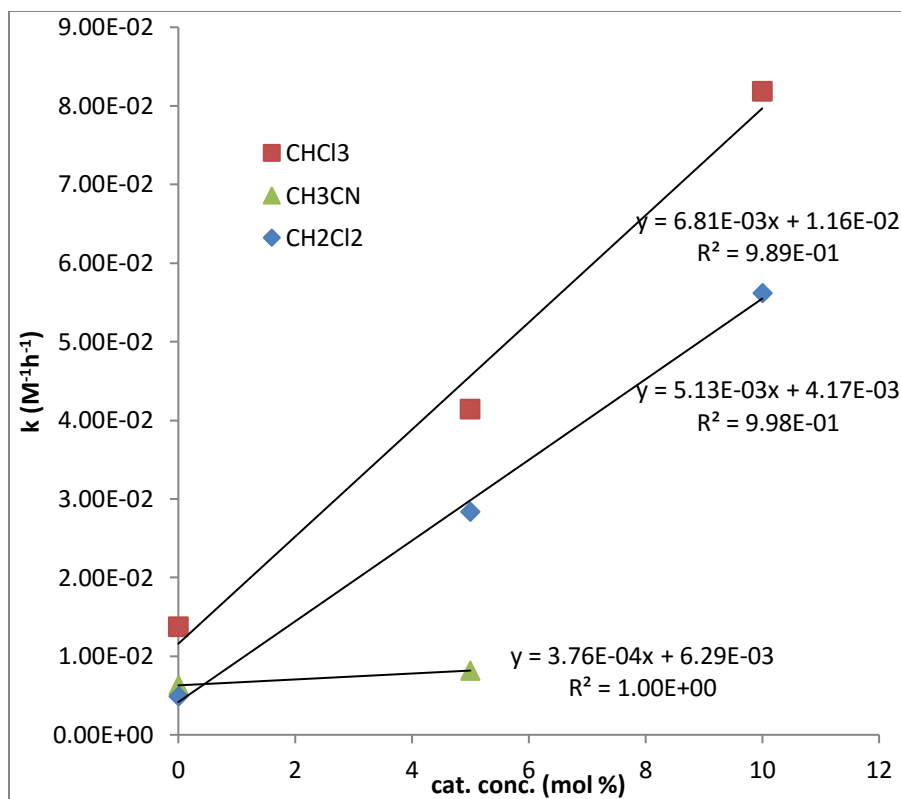


FIGURE 25: Relationship of the rate constant and catalyst concentration in chloroform, acetonitrile, and dichloromethane

This experiment suggests that the catalyst is most effective in chloroform, followed by dichloromethane, and the worst in acetonitrile. There are two potential active catalytic species: the monomer and dimer. If the catalyst is active as a monomer, the acetonitrile may be hydrogen bonding into the active site poisoning the catalyst inhibiting its activity. On the other hand if the catalyst is active as a dimer, there is a potential that acetonitrile prevents dimerization from occurring while chloroform and dichloromethane promote it (Figure 26).

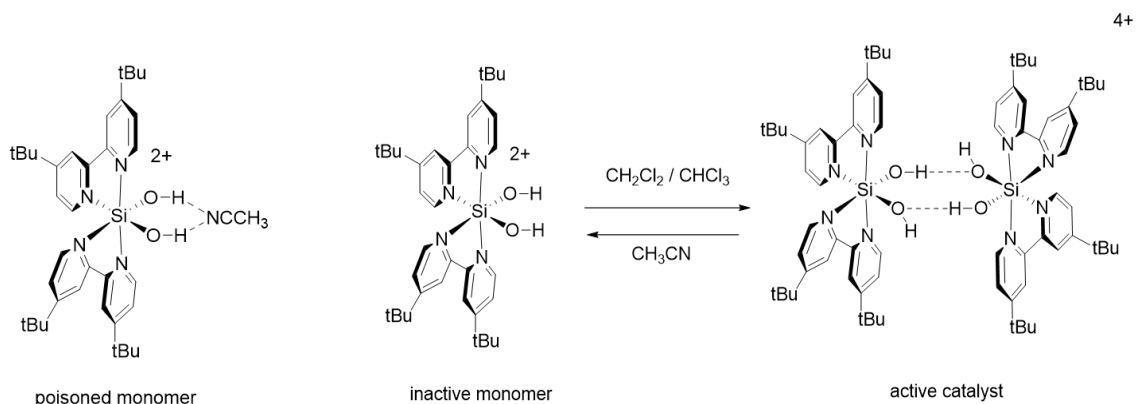


FIGURE 26: Possibilities of catalyst inhibition due to coordination of CD_3CN in the binding site or prevention of dimerization

After achieving positive results and proving that $[\text{Si}(\text{tBu}_2\text{bpy})_2(\text{OH})_2](\text{PF}_6)_2$ is a DHB that can catalyze the 1,4-conjugate addition test reaction of NMI to BNS, it was important to know if anything else in the reaction vessel may be causing the rate enhancement besides the silicon diol. To ensure no side reactions were occurring, the concentration of both the reactants, A and B, were monitored during the reaction progress. The sum of these reactants is plotted and the data is provided in Appendix C.

A major concern was the glass of the NMR tube, since it is made of silicon dioxide. A plastic NMR tube insert was used to see if there was a significant difference in the rate constant of the test reaction. The reaction was completed at 30 °C with 0 mol % catalyst loading. Because chloroform had the fastest uncatalyzed rate, this experiment was completed using the same reaction conditions as previously stated. It was determined that the difference was not large, but to ensure the glass had no effect on the catalysis results, all experiments were completed using a plastic NMR insert. A summary of the kinetic results are provided in Appendix D.

When the silicon diols are synthesized, Γ^- is the counterion. Before catalysis studies are completed, a metathesis reaction is used to exchange the counterion to a non-coordinating PF_6^- salt. To determine if a non-coordinating anion was necessary, the test reaction was completed with $[\text{Si}(\text{tBu}_2\text{bpy})_2(\text{OH})_2]\text{I}_2$ and $[\text{Si}(\text{tBu}_2\text{bpy})_2(\text{OH})_2](\text{PF}_6)_2$ at the 5 mol % catalyst loading. Figure 27 provides a summary of the data obtained.

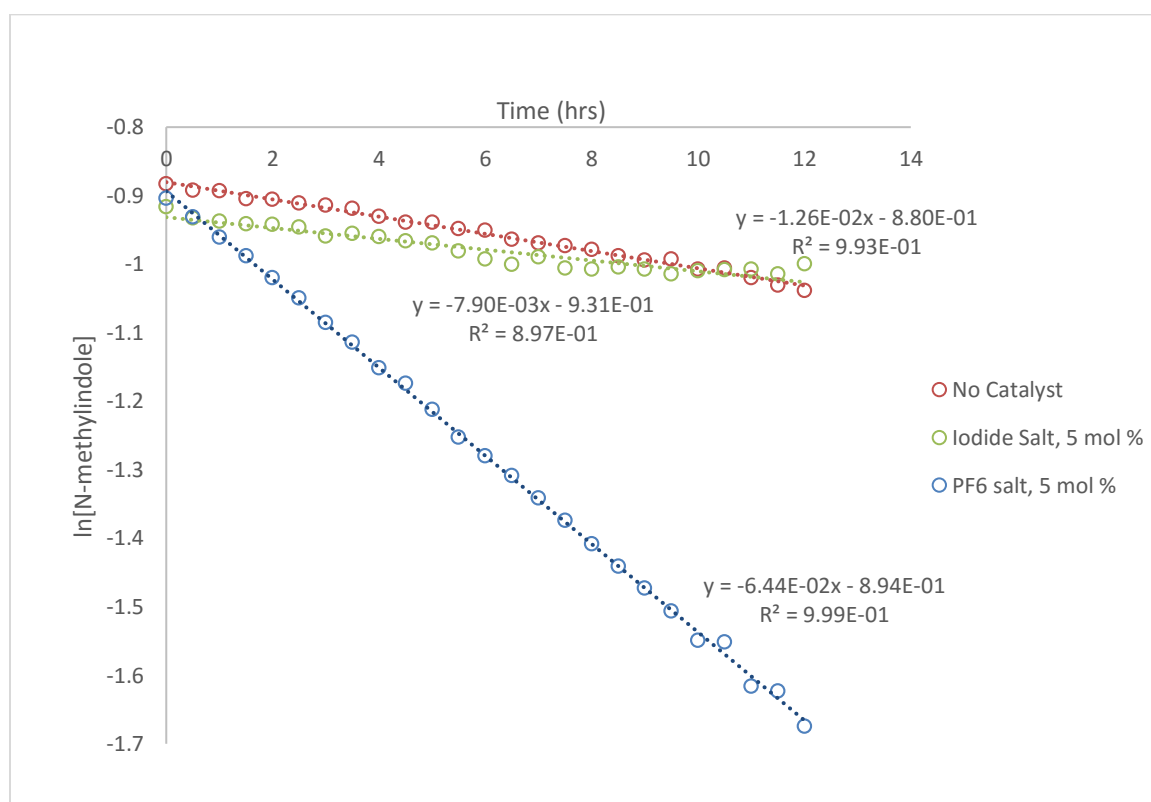


FIGURE 27: Comparison between the PF_6^- and Γ^- salt of $[\text{Si}(\text{tBu}_2\text{bpy})_2(\text{OH})_2]^{2+}$ in chloroform with 5 mol % catalyst loading

As shown by the slopes, the uncatalyzed rate is $k = 1.26 \times 10^{-2} \text{ M}^{-1}\text{hr}^{-1}$, the Γ^- salt has a rate of $k = 7.90 \times 10^{-3} \text{ M}^{-1}\text{hr}^{-1}$. The PF_6^- salt has a rate of $k = 6.44 \times 10^{-2} \text{ M}^{-1}\text{hr}^{-1}$. In Figure 27, it shows that the Γ^- salt seems to inhibit the catalyst making it proceed at a rate comparable to the uncatalyzed reaction.

This catalyst inhibition can be explained by two potential explanations. The catalyst as a monomeric species could be inhibited by the I⁻ coordinating to the diol, blocking the binding site. A crystal structure of [Si(Me₂bpy)₂(OH)₂]I₂, which is expected to be like the [Si(^tBu₂bpy)₂(OH)₂]I₂ in the solid state, is shown in Figure 28. The crystals were grown from an aqueous solution. The H-I bond length is 2.66 Å. The van der Waals radius of hydrogen and iodine is 1.20 Å and 1.98 Å, respectively. Because the H-I bond length is less than the sum of the radii of hydrogen and iodine, the data suggests that the I⁻ is in close enough proximity to hydrogen bond to the diol. If the active catalytic species is a dimer, the iodide may be preventing self-association of the diols inhibiting catalytic enhancement.

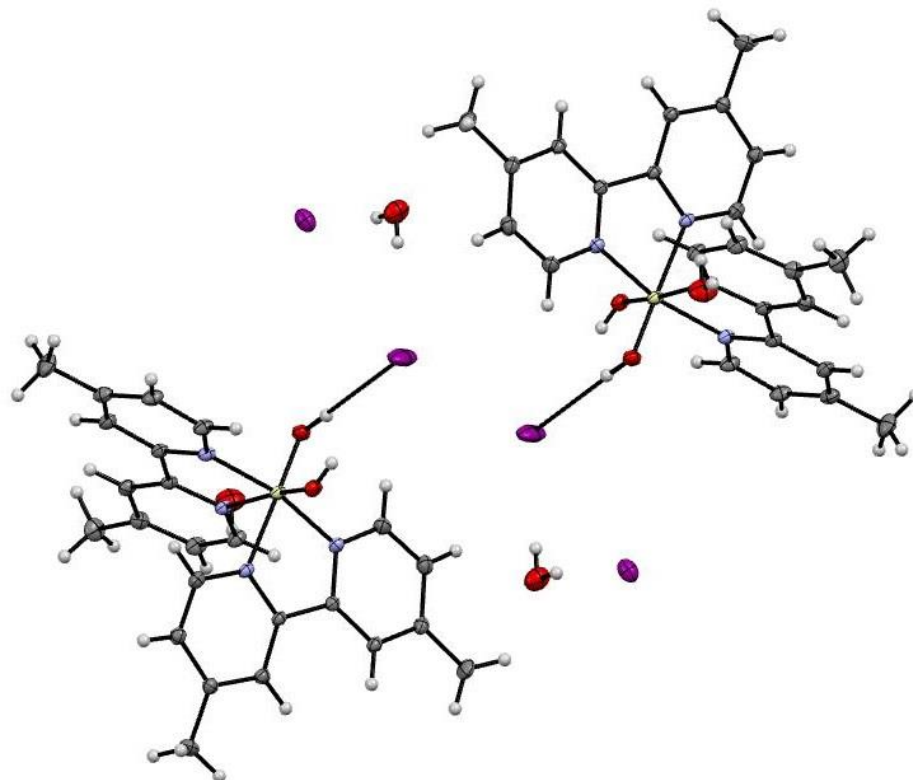


FIGURE 28: Crystal structure of $[\text{Si}(\text{Me}_2\text{bpy})_2(\text{OH})_2]\text{I}_2$ with a H-I bond length of 2.66 Å suggesting that hydrogen bonding is occurring

3.3.2 $[\text{Si}(\text{Me}_2\text{bpy})_2(\text{OH})_2](\text{PF}_6)_2$ as a DHB Catalyst

$[\text{Si}(\text{Me}_2\text{bpy})_2(\text{OH})_2](\text{PF}_6)_2$ was also used to determine if it had catalytic activity and how it compared to the $[\text{Si}(\text{tBu}_2\text{bpy})_2(\text{OH})_2](\text{PF}_6)_2$. The same test reaction (Scheme 2) of NMI to BNS in dichloromethane was completed to determine the rate constants.

Figure 29 provides the data obtained for the 5 and 10 mol % catalyst loading.

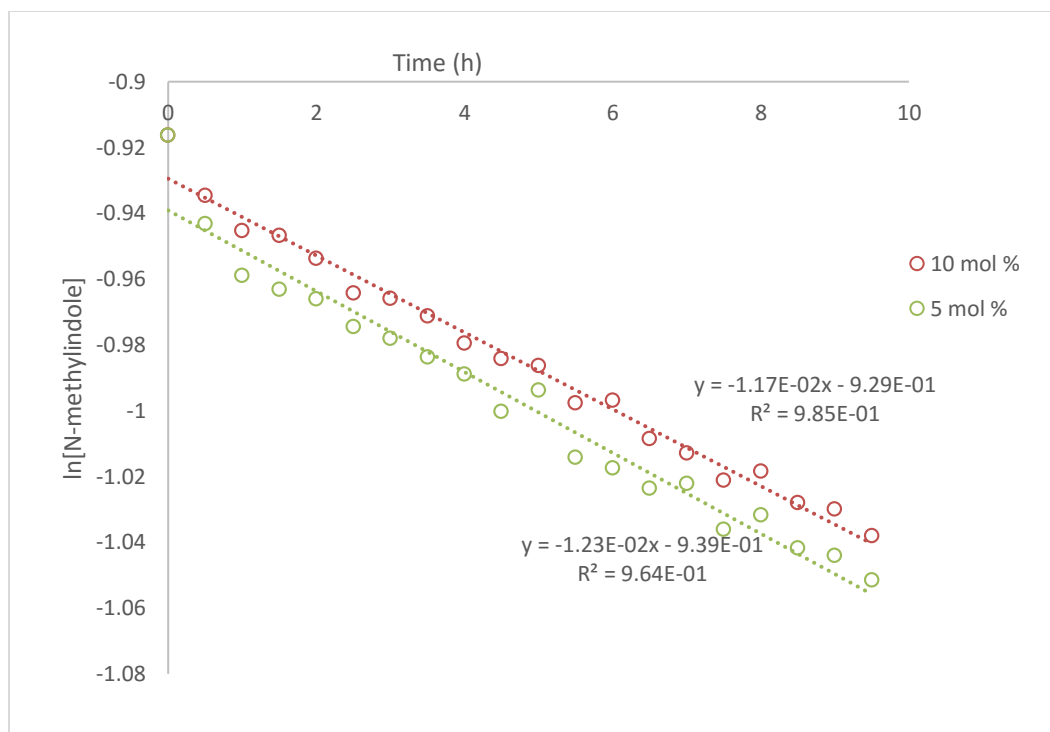


FIGURE 29: $[\text{Si}(\text{Me}_2\text{bpy})_2(\text{OH})_2](\text{PF}_6)_2$ rate constant determination at 5 and 10 mol % catalyst loading in DCM at 30 °C

The $[\text{Si}(\text{Me}_2\text{bpy})_2(\text{OH})_2](\text{PF}_6)_2$ yielded unexpected results. The 5 mol % catalyst loading had a k_{en} of 1.25 and the 10 mol % had a k_{en} of 1.44 which is a very small difference. The hypothesis was that since the $[\text{Si}(\text{tBu}_2\text{bpy})_2(\text{OH})_2](\text{PF}_6)_2$ behaved in a linear fashion, that the $[\text{Si}(\text{Me}_2\text{bpy})_2(\text{OH})_2](\text{PF}_6)_2$ would have a similar response. In this case, when there is a doubling of the catalyst loading, there is not a doubling in the enhanced rate. Using dichloromethane, the $[\text{Si}(\text{tBu}_2\text{bpy})_2(\text{OH})_2](\text{PF}_6)_2$ and all of the other reactants were totally soluble. With the $[\text{Si}(\text{Me}_2\text{bpy})_2(\text{OH})_2](\text{PF}_6)_2$ at 10 mol % loading, all of the reactants were soluble. A precipitate quickly formed during the addition of DCM to the reactants. At lower concentrations, the catalyst had excellent catalytic efficiency with almost a comparable rate enhancement as the $[\text{Si}(\text{tBu}_2\text{bpy})_2(\text{OH})_2](\text{PF}_6)_2$ at 5 mol %

catalyst loading. At higher concentrations, a solubility limit may be reached and therefore the minimalizing catalytic enhancement.

To determine the error associated with the kinetic results obtained in the project, it was expected that some error could arise from integration of the peak intensities of the ^1H NMR. To quantify this error, the 0 mol % catalyst loading in DCM was completed in triplicate. One data set was analyzed with three different integration ranges to estimate the error from solely integration. Results indicate that there is roughly a 7% relative standard deviation (RSD).

3.3.3 Experimental Error Analysis

To quantify the error within different experiments, four 0 mol % catalyst loading in DCM were completed and analyzed. An average of those four rate constants was calculated (Figure 30). The RSD was 22%.

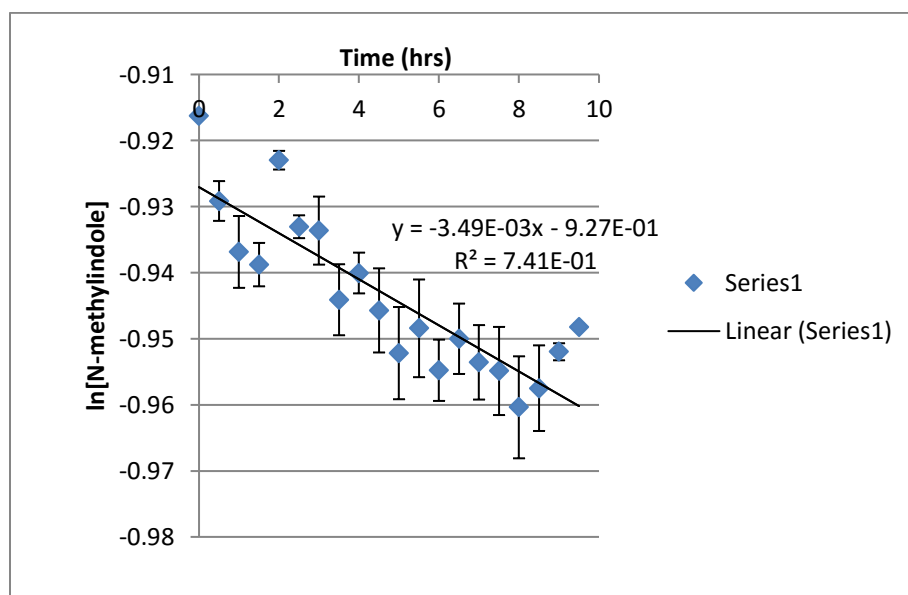


FIGURE 30: Error analysis within different experiments of the 0 mol % catalyst loading in DCM providing the averaged rate constant

3.4 Comparing Hexacoordinate Silicon Diols to a Tetracoordinate Silicon Diol

Hexacoordinate silicon diols are different from tetracoordinate silicon diols because they bear a charge. In neutral tetracoordinate species, it has been shown that self-association occurs forming a more acidic hydrogen making them better catalyst in the dimeric form. To determine how the hexacoordinate silicon diols compared to their tetracoordinate counterparts, the test reaction was completed with diphenyldihydroxysilane, $\text{Ph}_2\text{Si}(\text{OH})_2$, which is commercially available. $\text{Ph}_2\text{Si}(\text{OH})_2$ was added at 0, 5, 8, and 20 mol % catalyst loading (Figure 31).

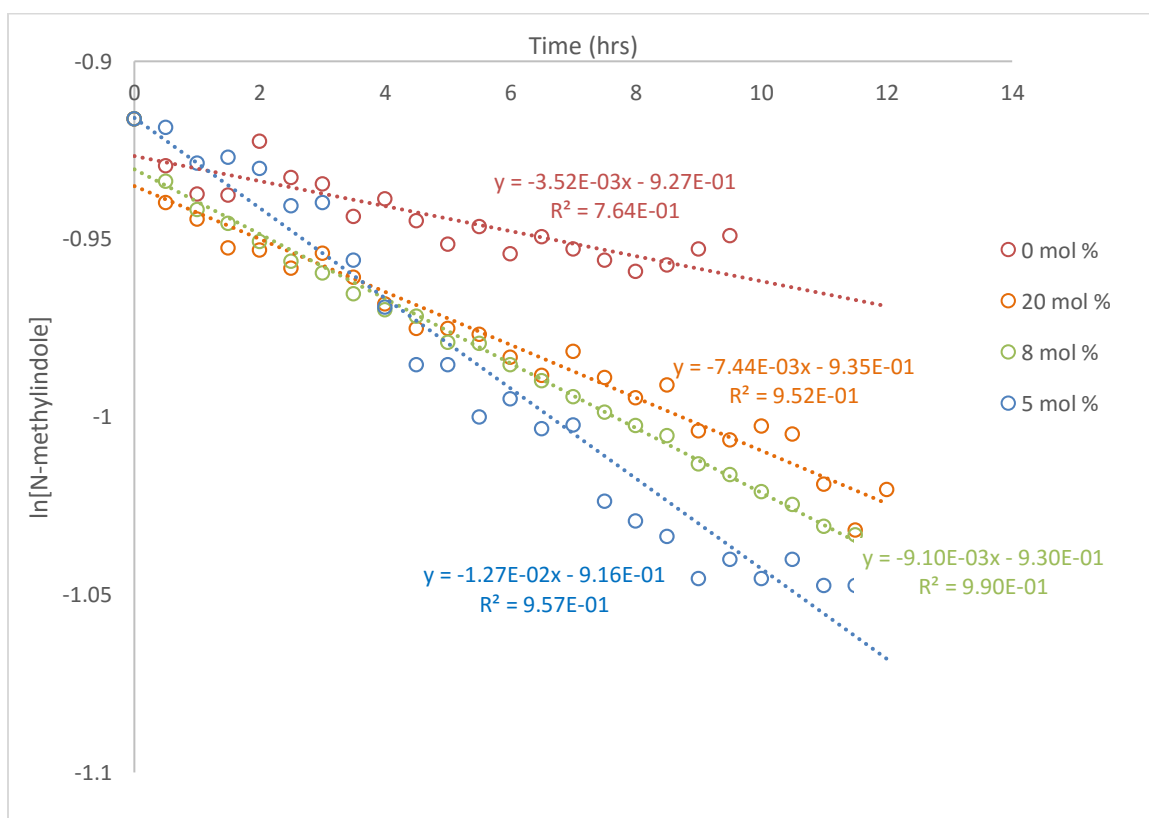


FIGURE 31: Diphenyldihydroxysilane at 0, 5, 8, and 20 mol % catalyst loading in DCM at 30 °C

At 5 and 10 mol % the k_{en} is 1.70 and 8.63, respectively. At these low mole percentages, $[\text{Si}(\text{tBu}_2\text{bpy})_2(\text{OH})_2](\text{PF}_6)_2$ outperforms the neutral $\text{Ph}_2\text{Si}(\text{OH})_2$ (Figure 32).

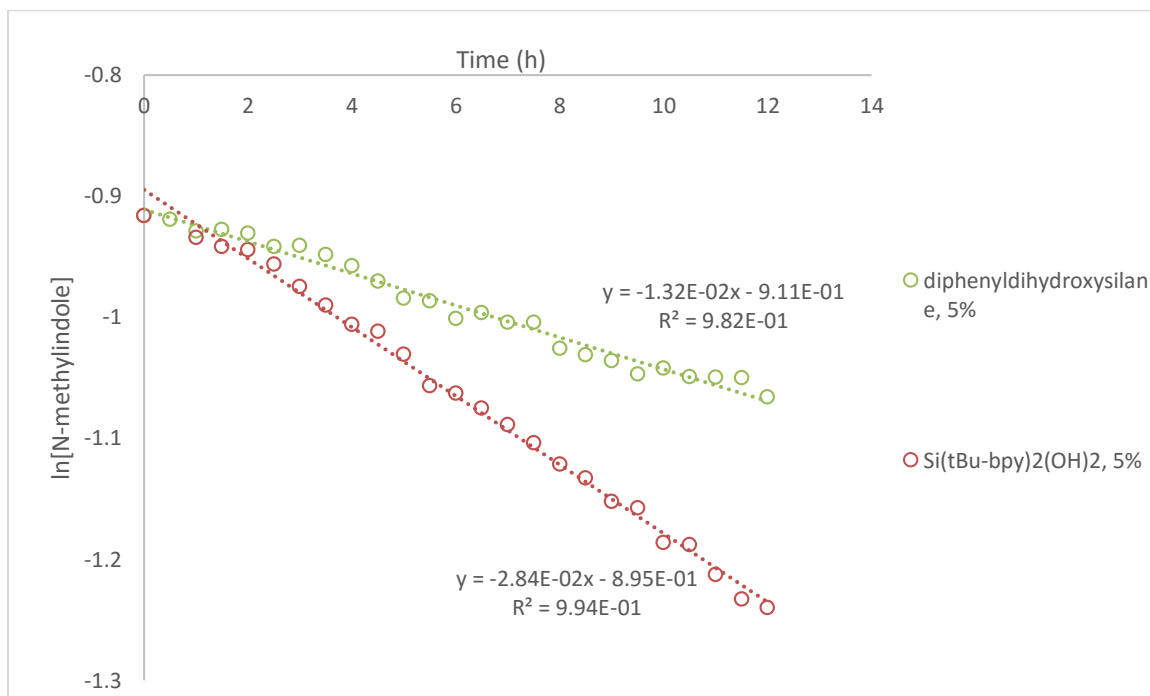


FIGURE 32: Comparison of $[\text{Si}(\text{tBu}_2\text{bpy})_2(\text{OH})_2](\text{PF}_6)_2$ and $\text{Ph}_2\text{Si}(\text{OH})_2$ at 5 mol % loading in DCM

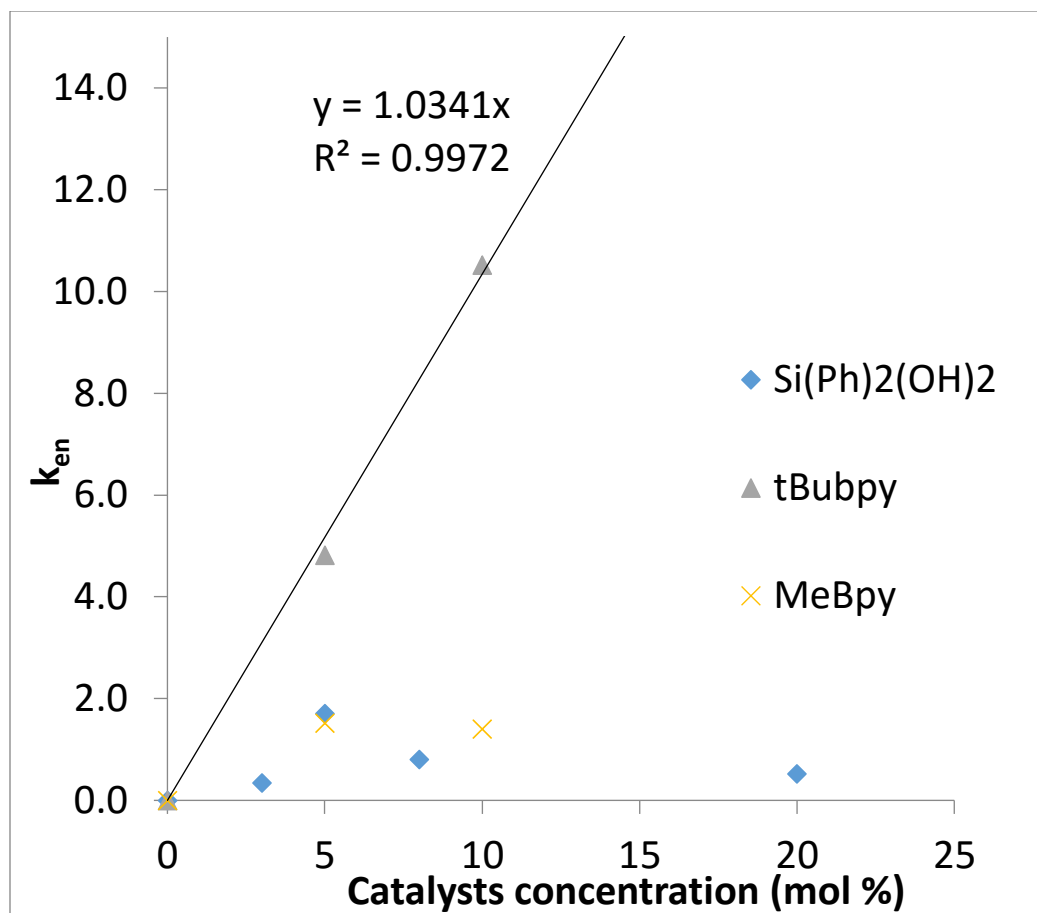


FIGURE 33: Relative enhanced rate of the silicon diols tested at the corresponding catalyst loading mole percentages

Figure 33 illustrates that there is no linear correlation with the $\text{Ph}_2\text{Si}(\text{OH})_2$ and $[\text{Si}(\text{Me}_2\text{bpy})_2(\text{OH})_2](\text{PF}_6)_2$. This means that when the catalyst concentration is doubled, there is not a doubling in the relative enhanced rate. With $[\text{Si}(\text{tBu}_2\text{bpy})_2(\text{OH})_2](\text{PF}_6)_2$, there is a linear response, hence the reason the slope of the linear regression is close to 1. When the concentration of the catalyst doubles, there is a doubling of the relative enhanced rate. This concludes that $[\text{Si}(\text{tBu}_2\text{bpy})_2(\text{OH})_2](\text{PF}_6)_2$ is a superior catalyst to the other two tested.

CHAPTER 4: EXPERIMENTAL DETAILS

4.1 General Synthesis Procedures

Silicon (IV) iodide was used and handled under nitrogen in a glove box or glove bag. All silicon diol syntheses were completed on a 0.500 gram or 1.00 gram scale. The ligands, 4,4'-bis(*tert*-butyl)-2,2'-bipyridine and 4,4'-dimethyl-2,2'-bipyridine, were purchased and were added to the SiI₄ in a 2.5 stoichiometric equivalence. Roughly 70 mL of chloroform was added to the ampoule along with a stir bar. The mixture was allowed to stir for 12 hours at 75 °C in an oil bath. Scheme 1 in Chapter 2 provides the synthesis route of the synthesized hexacoordinate silicon diols.

[Si(*t*Bu₂bpy)₂(OH)₂]I₂ Silicon(IV) iodide (0.500 g, 0.933 mmol), 4,4'-bis(*tert*-butyl)-2,2'-bipyridine (0.741 g, 2.76 mmol), and roughly 70 mL of chloroform were added to an ampoule inside of a glove box or glove bag, along with a stir bar. The sealed ampoule was allowed to react for 12 hours at 75 °C in an oil bath. The resulting suspension was separated using centrifugation and the separated solid was rinsed with chloroform. The resulting yellow solid was then washed with a copious amount of water, followed by diethyl ether. The precipitate was dried under vacuum for at least 12 hours. The I salt had a yield of 79%. C₃₆H₅₀N₄O₂I₂Si: ¹H NMR (CD₃CN, 300MHz): δ 1.34 (9H, s), 1.43 (9H, s), 9.49-9.48 (1H, d, J = 3.57 Hz), 8.76 (1H, s), 8.58 (1H, s), 8.20-8.19 (1H, d, J = 1.11 Hz), 7.49-7.48 (1H, d, J = 3.59 Hz), 7.03-7.02 (1H, d, J = 3.30 Hz).

[Si(*t*Bu₂bpy)₂(OH)₂](PF₆)₂ A metathesis reaction exchanges the counterion from I⁻ to PF₆⁻. It is converted to the PF₆⁻ salt by dissolving the compound in a 1:2 acetone mixture and 4 equivalents of ammonium hexafluorophosphate was added to the mixture after it had been dissolved in the minimum amount of water. The resulting product was rinsed with water to remove unreacted ammonium hexafluorophosphate and the sample was dried. The sample was then recrystallized from dichloromethane by diffusion of diethyl ether to provide x-ray quality crystals of [Si(*t*Bu₂bpy)₂(OH)₂](PF₆)₂·CH₃CH₂OCH₂CH₃. Attempts to remove the diethyl ether by overnight storage in an evacuated chamber was only partially successful. NMR experiments confirm sub-stoichiometric amounts of ether, and elemental analysis was consistent with a sample containing 0.35 molar equivalents of diethyl ether.

To obtain the ²⁹Si, Cr(acac)₃ was added to the sample to increase the relaxation time. A 60° pulse width was used with a relaxation delay of 10 s. ¹H NMR (CD₂Cl₂, 300 MHz): δ 1.61 (9H, s), 1.39 (9H, s), 9.62 (1H, d, J = 6.03 Hz), 8.56 (1H, s), 8.41 (1H, s), 8.15 (1H, d, J = 1.92 Hz), 7.62 (1H, d, J = 6.33 Hz), 7.07 (1H, d, J = 6.33 Hz). ¹³C{¹H} NMR (CD₂Cl₂, 125 MHz): δ 26.01 (1C, s), 36.5694 (1C, s), 37.18 (1C, s), 68.17 (1C, s), 120.81 (1C, s), 120.98 (1C, s), 127.11 (1C, s), 127.61 (1C, s), 142.46 (1C, s), 143.05 (1C, s), 144.43 (1C, s), 149.02 (1C, s), 170.09 (1C, s), 172.51 (1C, s). ²⁹Si NMR (CD₂Cl₂, 99 MHz): -156.04ppm. Anal. Calc. for C₃₆H₅₀N₄O₂P₂F₁₂Si·0.35(CH₃CH₂OCH₂CH₃): C, 49.11; H, 5.90; N, 6.13%; Found: C, 49.47; H, 6.09; N, 5.85%.

[Si(*Me*₂bpy)₂(OH)₂]I₂ Silicon (IV) iodide (1.03 g, 1.92 mmol), 4,4'-dimethyl-2,2'-bipyridine (1.50 g, 8.14 mmol), and roughly 70 mL of chloroform were added to an ampoule inside of a glove box, along with a stir bar. The sealed ampoule was then heated

in an oil bath at 75 °C for 12 hours. The resulting suspension was filtered using centrifugation and followed by rinsing with chloroform. The resulting yellow material was then washed with a copious amount of water followed by diethyl ether. The precipitate was then dried under vacuum for at least 12 hours. The I⁻ salt has a yield of 58.7%. Anal. Calc. for C₂₄H₂₆N₄O₂I₂Si: ¹H NMR (CD₃CN, 300 MHz): δ 2.50 (3H, s), 2.79 (3H, s), 9.49-9.48 (1H, d, J = 3.84 Hz), 8.72 (1H, s), 8.54 (1H, s), 8.03-8.02 (1H, d, J = 3.84 Hz), 7.36-7.35 (1H, d, J = 3.30 Hz), 7.01-6.99 (1H, d, J = 3.57 Hz).

[Si(Me₂bpy)₂(OH)₂](PF₆)₂ The crude product was converted to the PF₆⁻ salt by dissolving the compound in a 1:2 water to acetone mixture and 4 equivalents of ammonium hexafluorophosphate was added to the mixture after it had been dissolved in the minimum amount of water. The resulting procedure was rinsed with water to remove unreacted ammonium hexafluorophosphate and the sample was dried overnight. NMR and elemental analysis are both consistent with the monohydrate,

[Si(Me₂bpy)₂(OH)₂](PF₆)₂·H₂O. ¹H NMR (CD₃CN, 500 MHz): δ 2.50 (3H, s), 2.79 (3H, s), 3.84 (1H, s), 6.95-6.97 (1H, d, J = 10.05 Hz), 7.33-7.36 (1H, d, J = 11.00 Hz), 8.01-8.03 (1H, d, J = 10.10 Hz), 8.41 (1H, s), 8.60 (1H, s), 9.43-9.45 (1H, d, J = 10.50 Hz). Anal. Calc. for C₂₄H₂₆N₄O₂P₂F₁₂Si·H₂O: C, 39.03; H, 3.82; N, 7.59%; Found: C, 39.23; H, 4.04; N, 7.61%.

2-(N-methylindolyl)-2-phenyl-1-nitroethane. This is the addition product that was formed during the kinetic experiments. The ¹H and ¹³C NMR data is provided to ensure the correct intensity was integrated for determining catalytic enhancement. ¹H NMR (400 MHz, CDCl₃) δ 7.39–6.93 (m, 9H), 6.67 (s, 1H), 5.06 (dd, J=8.72, 7.92 Hz, 1H), 4.83 (dd, J=12.32, 7.92 Hz, 1H), 4.76 (dd, J=12.32, 8.72 Hz, 1H), 3.14 (s, 3H). ¹³C NMR

(100 MHz, CDCl₃) δ 139.31, 136.99, 128.59, 127.49, 127.19, 126.32, 126.07, 121.89, 119.15, 118.71, 112.43, 109.33, 79.19, 41.23, 32.24.

4.2 NMR Kinetic Experiments

The 1,4-conjugate addition reaction was completed under pseudo-first order conditions with respect to NMI. BNS was in excess at 4 M (0.600 grams). NMI was 0.4 M (51 μ L) and a stoichiometric mole percent of catalyst, with respect to NMI, was added. The solvent was used to dilute the mixture to 1 mL. The experiments were completed using a JEOL 300 MHz or JEOL 500 MHz NMR. A single pulse experiment was used to collect 8 scans every thirty minutes for 10-12 hours. The reaction was completed in a plastic NMR insert to eliminate the glass from potentially catalyzing the reaction. The reaction progress was monitored by integrating the intensity of the N-methyl peak of the reactant and product.

4.3 Chiral Chromatography

[Si(^tBu₂bp_y)₂(OH)₂]₂I₂ Chiral Resolutions

A column with a length of 15 mL of Sephadex was prepared by pouring a slurry solution in water into the buret. A 0.52 M Na[Sb(tartrate)] aqueous solution was used as the mobile phase. The mobile phase was flushed through the column for about 5 mins prior to the first loading of [Si(^tBu₂bp_y)₂(OH)₂]₂I₂. About 3-5 mg of the diol was dissolved in 5 mL of water. A flow cell was used to determine when the compound eluted the column. A polychromator was used to monitor the elution of the compound from the column.

Once the compound was collected from the column, it was tested for enantiomeric enrichment using the spectropolarimeter. There was no success in enantiomeric resolution using this method.

[Si(Me₂bpy)₂(OH)₂]₂I₂ Chiral Resolutions

A 1 mL pipette column was used to resolve the enantiomers of the [Si(Me₂bpy)₂(OH)₂]₂I₂ compound. A slurry solution of Sephadex in water was used to pack the column. A 0.52 M solution of Na[Sb(tartrate)] was used to elute the compound. Fractions were collected in 1 mL increments and tested using the spectropolarimeter for enantiomeric enrichment. The enantiomers were separated, but due to the small concentration of the material loaded on the column, none could be recovered for kinetic experiments.

CHAPTER 5: CONCLUSIONS AND FUTURE DIRECTIONS

5.1 Conclusions

Bis(bipyridyl)silicon(IV) diols have been shown to exhibit catalytic activity. Two diols were synthesized, $[\text{Si}(\text{Me}_2\text{bpy})_2(\text{OH})_2]^{2+}$ and $[\text{Si}(\text{tBu}_2\text{bpy})_2(\text{OH})_2]^{2+}$. It is still unknown whether these compounds are catalytically active as monomers or dimers. It was determined that $[\text{Si}(\text{tBu}_2\text{bpy})_2(\text{OH})_2]^{2+}$ has superior catalytic properties over other silicon diols that were tested. When the catalyst loading doubled, the enhanced rate also doubled. This positive, linear trend was not present for the other two catalyst tested.

To optimize the catalyst, solvent effects were analyzed. The 1,4-conjugate addition reaction of NMI to BNS was completed in three different solvents and it was determined that chloroform and dichloromethane promote catalytic efficiency whereas acetonitrile caused catalytic inhibition. This inhibition was caused through either prevention of dimerization or poisoning of the monomer through coordination of the solvent. Because DHBs are likely to hydrogen bond to anions, non-coordinating anions are necessary for catalytic testing. Testing the I^- salt showed that the iodide ion inhibits catalytic activity by hydrogen bonding into the binding site of a monomeric catalyst, or inhibiting dimerization from occurring.

Resolution of the enantiomers of the $[\text{Si}(\text{Me}_2\text{bpy})_2(\text{OH})_2]^{2+}$ has been shown, but racemization rate is an urgent question to explore. While this compound has been

resolved, the $[\text{Si}(\text{tBu}_2\text{bpy})_2(\text{OH})_2]^{2+}$ has not. Further experiments could be completed to determine if chiral catalysis is a possible avenue for these hexacoordinate silicon diols.

5.2 Future Directions

5.2.1 Rate Determination of Other Reactions Using Silicon Diols

In this project, only two silicon diols were experimentally tested to determine the rate constant of the 1,4-conjugate addition reaction of NMI to BNS. The scope of these compounds can be expanded even more. A repertoire of hexacoordinate silicon diols can be synthesized (Figure 33) and the catalytic efficiency of each can be determined.

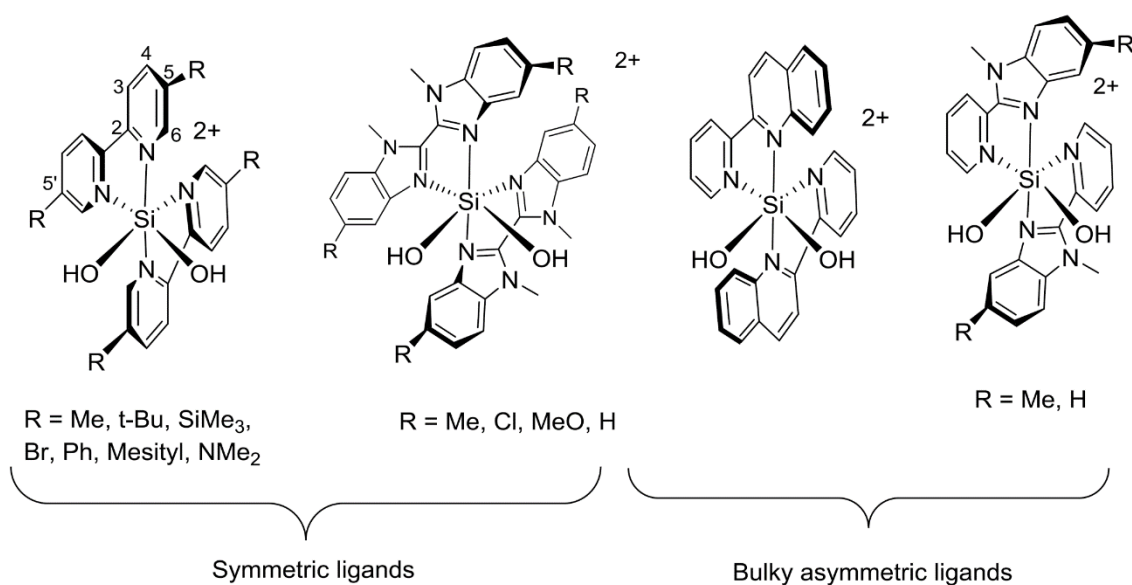


FIGURE 34: Potential symmetric and bulky asymmetric ligands that can be used to expand hexacoordinate silicon diols

Other diols to be considered are symmetric ligands, such as the 5,5'-substituted 2,2'-bipyridine ligand and bis-benzimidazole ligands. R groups can be manipulated to change the chiral binding site where hydrogen bonding and electrophilic activation is occurring. The symmetric ligands have a more direct synthesis route and will probably be easier to

synthesize than the asymmetric ligands. The reason asymmetric ligands are promising is because of the C_2 rotation axis of the hexacoordinate silicon diol. Both sides of the ligand do not need to have steric bulk to dictate the chiral binding site of the diol. The asymmetric ligands are going to be more difficult to synthesize, but a good avenue to explore when building a repertoire of silicon diols.

DHBs were shown to catalyze two types of organic reactions: 1,4-conjugate addition and the Diels-Alder reaction. In this study, only one of the two test reactions was explored to determine if the silicon diols were catalytically active. A Diels-Alder reaction needs to be tested to determine if the silicon diols are equally as efficient at catalyzing the reaction. The test reaction can be monitored using 1H NMR and quantifying the rate constant by integrating the peaks, similarly to what was completed experimentally in this project.

5.2.2 Chiral Catalysis using Hexacoordinate Silicon Diols

Hexacoordinate silicon diols have the ability to be chiral because of a C_2 rotation axis.

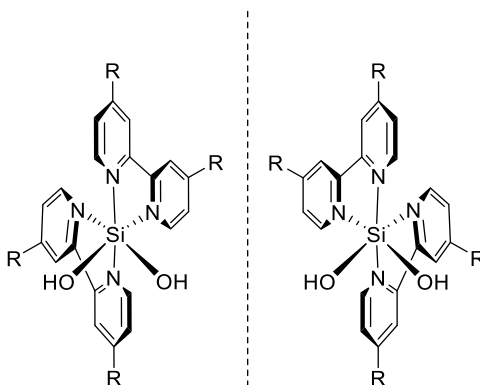


FIGURE 35: Two enantiomers of the 4,4' substituted 2,2'-bipyridine silicon diols

The Ohmori group determined that $[\text{Si}(\text{bpy})_2(\text{OH})_2]^{2+}$ could be enantiomerically separated using a fractional crystallization method.⁴⁵ A similar method could be applied in attempts to separate the enantiomers of the two diols that were developed in this project. Even though efforts were made toward the separation using fractional crystallization and column chromatography, no chiral catalysis was tested. Once the diol has been separated into its two enantiomers, it must undergo a metathesis reaction to swap the tartrate salt back to the PF_6^- salt. Catalysis can be completed using the same test reaction followed by spectropolarimetry. Spectropolarimetry will allow any enantiomeric excess to be quantified.

Using the 5,5' substituted bipyridine ligand on the hexacoordinate diol may lead to greater enantioselectivity. With the way the diol rotates, depending on the enantiomer chosen, one of the enantiomers will promote only nucleophilic attack from one side of the electrophile. Figure 35 shows the 5,5'-bis(*tert*-butyl)-2,2'-bipyridinesilicon(IV) diol hydrogen bonding to a 2-cyclo-hexen-1-one. One side of the electrophile is obstructed so that only one face is available for attack.

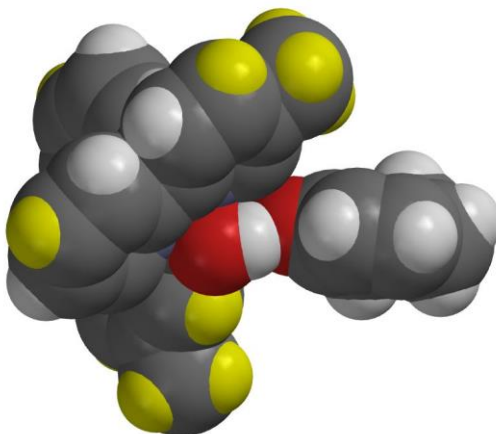


FIGURE 36: Spartan calculated space filling of 5,5'-bis(*tert*-butyl)-2,2'-bipyridinesilicon(IV) diol coordinated to a 2-cyclohexen-1-one through cooperative hydrogen bonding

5.2.3 Using Silicon Triols as Polyols for Hydrogen Bond Catalysis

Silicon triols and other polyols have recently become another avenue to explore for HBD catalysis.^{49,50,51} One of the major issue with silicon triols is their stability. Because of the hydroxyl groups self-condensation reactions (elimination of water) readily occur, degrading these compounds. Silicon triols need to be stabilized using bulky substituents because they inhibit the triol from self-condensation reactions.⁵² Once the triols are synthesized, they need to be fully characterized and then the catalytic ability can be determined. It can be hypothesized that silicon triols would have a greater catalytic efficiency than the diols because there are now three sites for hydrogen bonding to occur. If the catalyst acts as a monomer, dimerization would not inhibit the catalyst because there was still be a remaining site for electrophilic activation through hydrogen bonding. Examples of potential silicon triols are found in Figure 37.

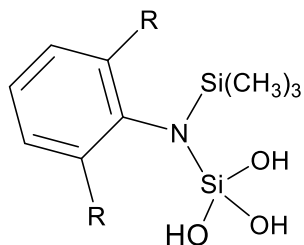


FIGURE 37: Example of a known silicon triol⁵³

5.2.4 Multi-functional Asymmetric Catalysis

Few groups have started looking towards multi-functional asymmetric catalysis.^{54,55,56} Hexacoordinate silicon diols can also potentially be asymmetric multi-functional catalysts.

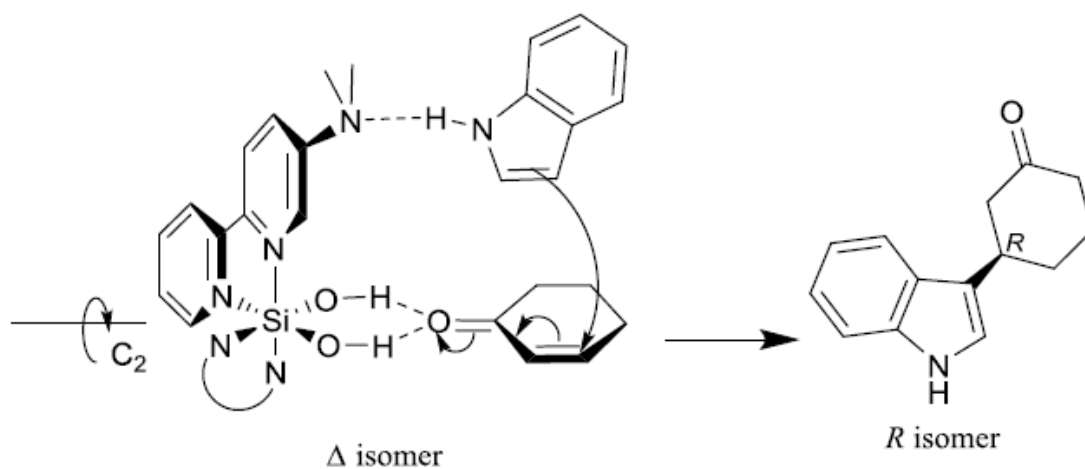


FIGURE 38: Hexacoordinate silicon diols activating an electrophile and a nucleophile simultaneously promoting a chiral addition product

The hydrogen bond site is activating the cyclohexen-1-one for nucleophilic attack while the Lewis basic site of the ligand activates the nucleophile. Because there is a chiral binding site, the product is enantiomerically enriched.

REFERENCES

1. Uraguchi, D.; Terada, M., Chiral Bronsted acid-catalyzed direct Mannich reactions via electrophilic activation. *J. Am. Chem. Soc.* **2004**, *126*, 5356-7.
2. Akiyama, T.; Morita, H.; Fuchibe, K., Chiral Bronsted acid-catalyzed inverse electron-demand aza Diels-Alder reaction. *J. Am. Chem. Soc.* **2006**, *128*, 13070-1.
3. McDougal, N. T.; Schaus, S. E., Asymmetric Morita-Baylis-Hillman reactions catalyzed by chiral Bronsted acids. *J. Am. Chem. Soc.* **2003**, *125*, 12094-5.
4. Terada, M.; Sorimachi, K., Enantioselective Friedel-Crafts reaction of electron-rich alkenes catalyzed by chiral Bronsted acid. *J. Am. Chem. Soc.* **2007**, *129*, 292-3.
5. Rueping, M.; Sugiono, E.; Azap, C.; Theissmann, T.; Bolte, M., Enantioselective Bronsted acid catalyzed transfer hydrogenation: organocatalytic reduction of imines. *Org. Lett.* **2005**, *7*, 3781-3.
6. Nakashima, D.; Yamamoto, H., Design of chiral N-triflyl phosphoramidate as a strong chiral Bronsted acid and its application to asymmetric Diels-Alder reaction. *J. Am. Chem. Soc.* **2006**, *128*, 9626-7.
7. Guo, Q. X.; Liu, H.; Guo, C.; Luo, S. W.; Gu, Y.; Gong, L. Z., Chiral Bronsted acid-catalyzed direct asymmetric Mannich reaction. *J. Am. Chem. Soc.* **2007**, *129*, 3790-1.
8. Nugent, B. M.; Yoder, R. A.; Johnston, J. N., Chiral proton catalysis: a catalytic enantioselective direct aza-Henry reaction. *J. Am. Chem. Soc.* **2004**, *126*, 3418-9.
9. Bah, J.; Franzen, J., Carbocations as Lewis acid catalysts in Diels-Alder and Michael addition reactions. *Chem. Eur. J.* **2014**, *20*, 1066-72.
10. Wabnitz, T. C.; Yu, J. Q.; Spencer, J. B., Evidence that protons can be the active catalysts in Lewis acid mediated hetero-Michael addition reactions. *Chem. Eur. J.* **2004**, *10*, 484-93.
11. Johnston, J. N.; Evans, D. A.; Willis, M. C., Catalytic Enantioselective Michael Additions to Unsaturated Ester Derivatives Using Chiral Copper(II) Lewis Acid Complexes. *Org. Lett.* **1999**, *1*, 865-868.
12. Otto, S.; Boccaletti, G.; Engberts, J. B. F. N., A Chiral Lewis-Acid-Catalyzed Diels-Alder Reaction. Water-Enhanced Enantioselectivity. *J. Am. Chem. Soc.* **1998**, *120*, 4238-4239.

13. (a) Ahrendt, K. A.; Borths, C. J.; MacMillan, D. W. C., New Strategies for Organic Catalysis: The First Highly Enantioselective Organocatalytic Diels–Alder Reaction. *J. Am. Chem. Soc.* **2000**, *122*, 4243-4244; (b) Houk, K. N.; Strozier, R. W., Lewis acid catalysis of Diels–Alder reactions. *J. Am. Chem. Soc.* **1973**, *95*, 4094-4096.
14. Gatzenmeier, T.; van Gemmeren, M.; Xie, Y.; Hofler, D.; Leutzsch, M.; List, B., Asymmetric Lewis acid organocatalysis of the Diels–Alder reaction by a silylated C–H acid. *Science* **2016**, *351*, 949-52.
15. Kobayashi, S.; Manabe, K., Development of Novel Lewis Acid Catalysts for Selective Organic Reactions in Aqueous Media. *Acc. Chem. Res.* **2002**, *35*, 209-217.
16. Akiyama, T., Stronger Bronsted acids. *Chem. Rev.* **2007**, *107*, 5744-58.
17. Shen, X.; Huo, H.; Wang, C.; Zhang, B.; Harms, K.; Meggers, E., Octahedral Chiral-at-Metal Iridium Catalysts: Versatile Chiral Lewis Acids for Asymmetric Conjugate Additions. *Chem. Eur. J.* **2015**, *21*, 9720-6.
18. Wang, C.; Chen, L.-A.; Huo, H.; Shen, X.; Harms, K.; Gong, L.; Meggers, E., Asymmetric Lewis acid catalysis directed by octahedral rhodium centrochirality. *Chem. Sci.* **2015**, *6*, 1094-1100.
19. Taylor, M. S.; Jacobsen, E. N., Asymmetric catalysis by chiral hydrogen-bond donors. *Angew. Chem. Int. Ed. Engl.* **2006**, *45*, 1520-43.
20. Trylska, J.; Grochowski, P.; McCammon, J. A., The role of hydrogen bonding in the enzymatic reaction catalyzed by HIV-1 protease. *Protein Sci.* **2004**, *13*, 513-28.
21. Simon, L.; Goodman, J. M., Enzyme catalysis by hydrogen bonds: the balance between transition state binding and substrate binding in oxyanion holes. *J. Org. Chem.* **2010**, *75*, 1831-40.
22. White, A. J.; Wharton, C. W., Hydrogen-bonding in enzyme catalysis. Fourier-transform infrared detection of ground-state electronic strain in acyl-chymotrypsins and analysis of the kinetic consequences. *Biochem. J.* **1990**, *270*, 627-37.
23. Akiyama, T.; Itoh, J.; Yokota, K.; Fuchibe, K., Enantioselective Mannich-type reaction catalyzed by a chiral Bronsted acid. *Angew. Chem. Int. Ed. Engl.* **2004**, *43*, 1566-8.
24. Rueping, M.; Uria, U.; Lin, M. Y.; Atodiresei, I., Chiral organic contact ion pairs in metal-free catalytic asymmetric allylic substitutions. *J. Am. Chem. Soc.* **2011**, *133*, 3732-5.
25. Scherer, A.; Mukherjee, T.; Hampel, F.; Gladysz, J. A., Metal-Templated Hydrogen Bond Donors as "Organocatalysts" for Carbon–Carbon Bond Forming

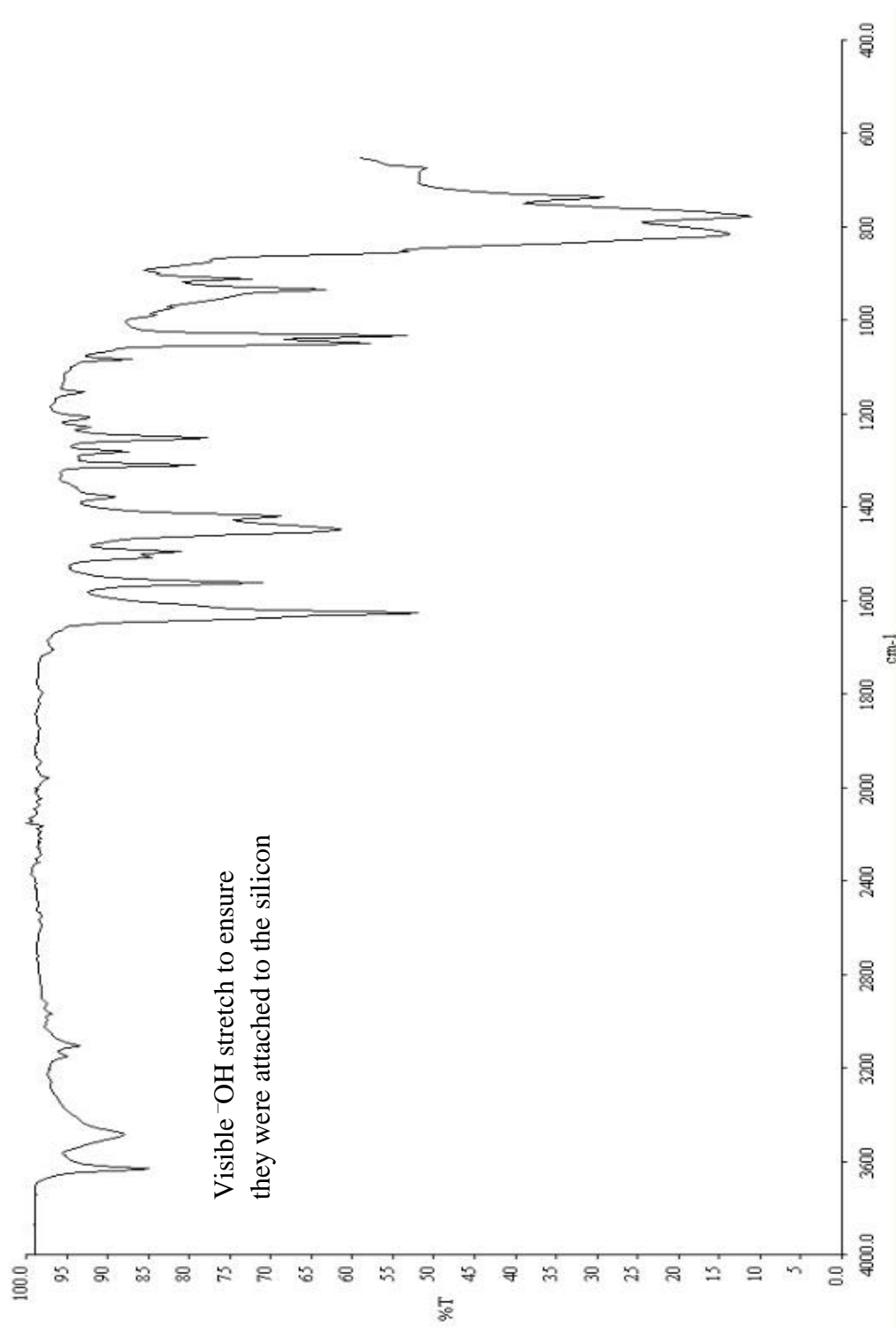
Reactions: Syntheses, Structures, and Reactivities of 2-Guanidinobenzimidazole Cyclopentadienyl Ruthenium Complexes. *Organometallics* **2014**, *33*, 6709-6722.

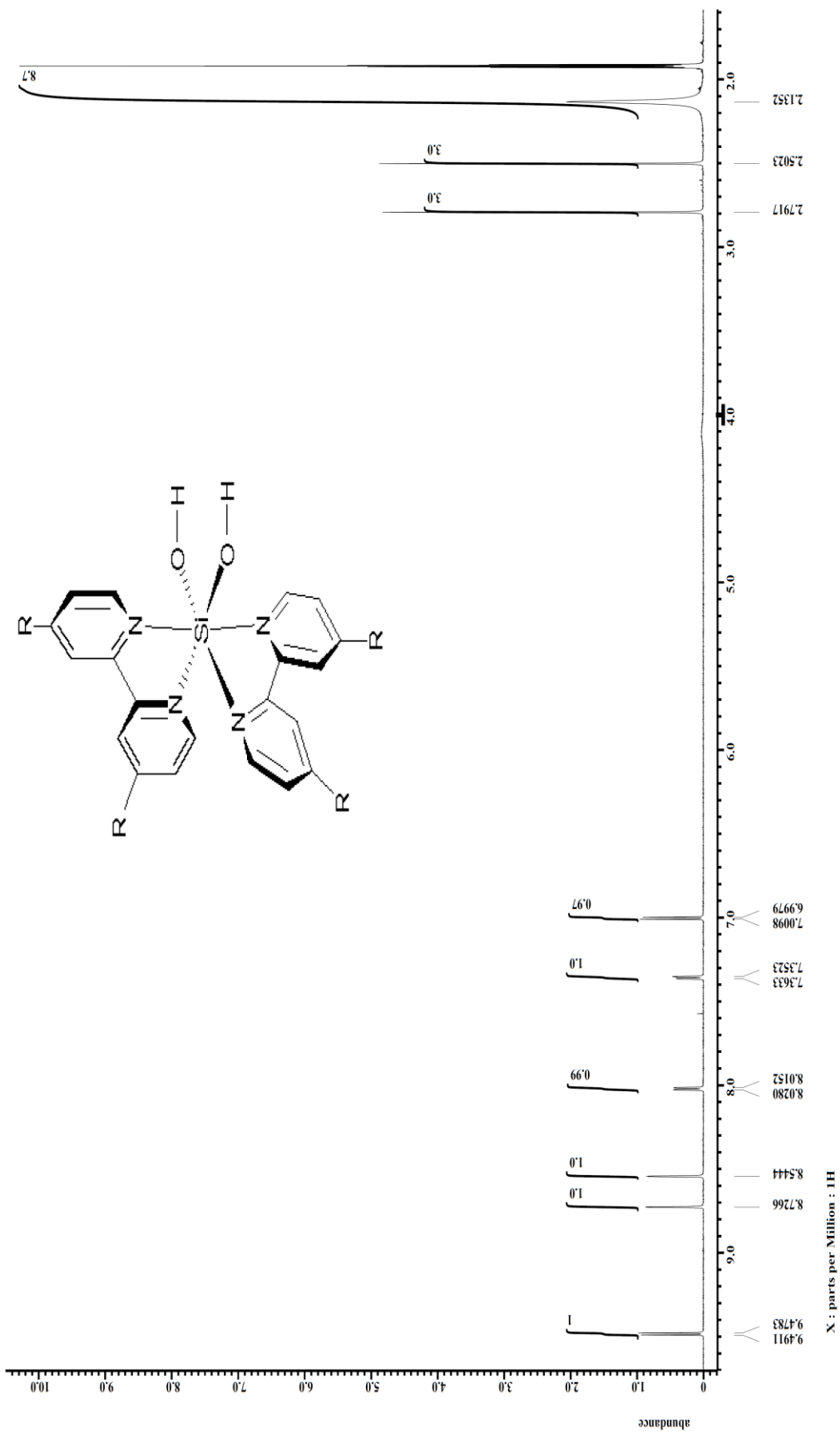
26. Tang, W.; Johnston, S.; Li, C.; Iggo, J. A.; Bacsá, J.; Xiao, J., Cooperative catalysis: combining an achiral metal catalyst with a chiral Bronsted acid enables highly enantioselective hydrogenation of imines. *Chem. Eur. J.* **2013**, *19*, 14187-93.
27. Walvoord, R. R.; Huynh, P. N.; Kozłowski, M. C., Quantification of electrophilic activation by hydrogen-bonding organocatalysts. *J. Am. Chem. Soc.* **2014**, *136*, 16055-65.
28. Akiyama, T.; Itoh, J.; Fuchibe, K., Recent progress in chiral Bronsted acid catalysis. *Adv. Synth. Catal.* **2006**, *348*, 999-1010.
29. Doyle, A. G.; Jacobsen, E. N., Small-molecule H-bond donors in asymmetric catalysis. *Chem. Rev.* **2007**, *107*, 5713-43.
30. Hesticová, M.; Šebesta, R., Higher enantioselectivities in thiourea-catalyzed Michael additions under solvent-free conditions. *Tetrahedron* **2014**, *70*, 901-905.
31. Ganesh, M.; Seidel, D., Catalytic enantioselective additions of indoles to nitroalkenes. *J. Am. Chem. Soc.* **2008**, *130*, 16464-5.
32. Takenaka, N.; Chen, J.; Captain, B.; Sarangthem, R. S.; Chandrakumar, A., Helical chiral 2-aminopyridinium ions: a new class of hydrogen bond donor catalysts. *J. Am. Chem. Soc.* **2010**, *132*, 4536-7.
33. Chandrasekhar, V.; Boomishankar, R.; Nagendran, S., Recent developments in the synthesis and structure of organosilanols. *Chem. Rev.* **2004**, *104*, 5847-910.
34. Schon, E. M.; Marques-Lopez, E.; Herrera, R. P.; Aleman, C.; Diaz Diaz, D., Exploiting molecular self-assembly: from urea-based organocatalysts to multifunctional supramolecular gels. *Chem. Eur. J.* **2014**, *20*, 10720-31.
35. Tran, N. T.; Min, T.; Franz, A. K., Silanediol hydrogen bonding activation of carbonyl compounds. *Chem. Eur. J.* **2011**, *17*, 9897-900.
36. Mutahi, M. w.; Nittoli, T.; Guo, L.; Sieburth, S. M., Silicon-Based Metalloprotease Inhibitors: Synthesis and Evaluation of Silanol and Silanediol Peptide Analogues as Inhibitors of Angiotensin-Converting Enzyme1. *J. Am. Chem. Soc.* **2002**, *124*, 7363-7375.
37. Shumaila, A. M. A.; Kusurkar, R. S., Silica Gel, an Effective Catalyst for the Reaction of Electron-Deficient Nitro-Olefins with Nitrogen Heterocycles. *Syn. Comm.* **2010**, *40*, 2935-2940.

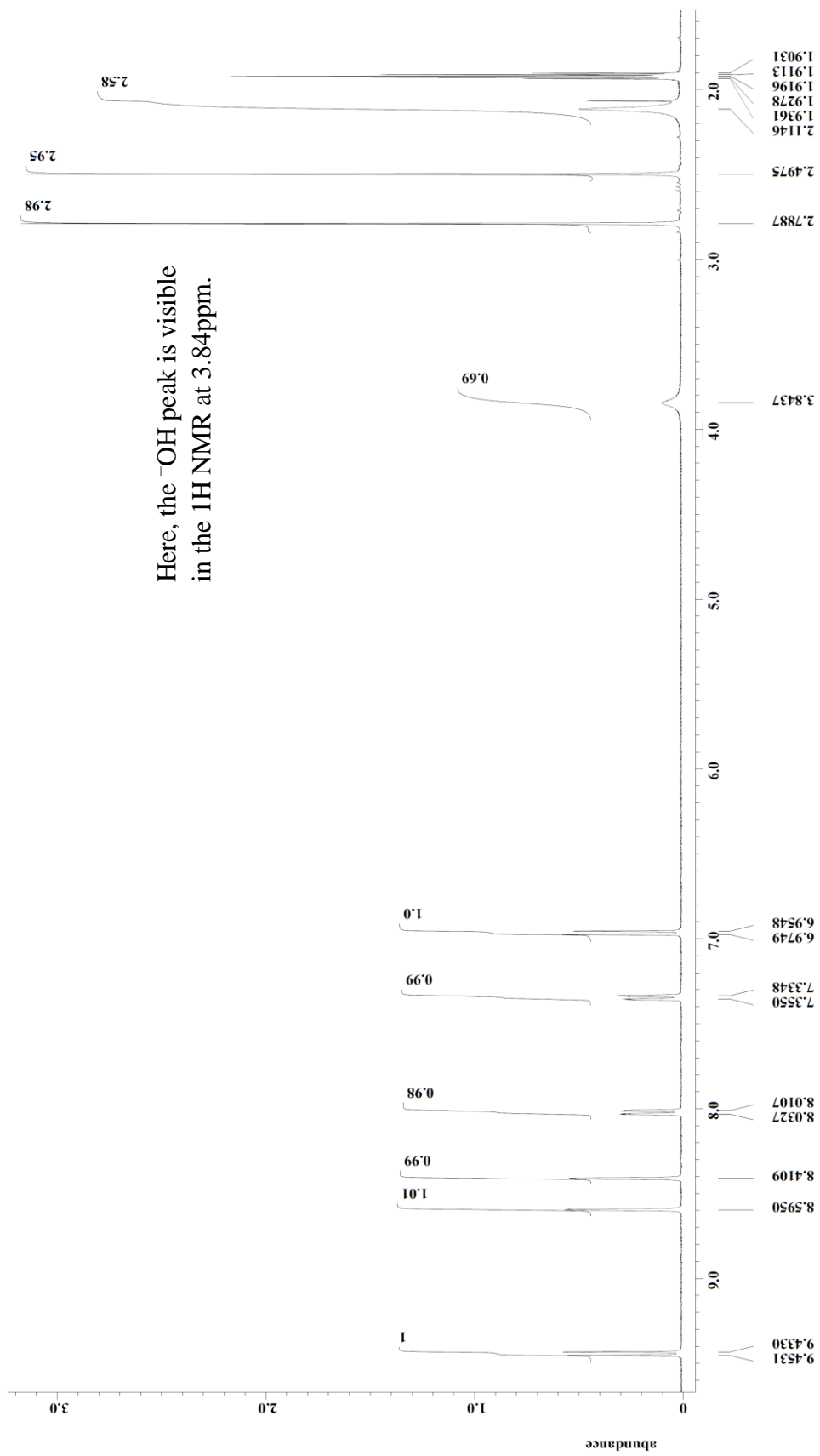
38. Schafer, A. G.; Wieting, J. M.; Mattson, A. E., Silanediols: a new class of hydrogen bond donor catalysts. *Org. Lett.* **2011**, *13*, 5228-31.
39. Kondo, S.; Harada, T.; Tanaka, R.; Unno, M., Anion recognition by a silanediol-based receptor. *Org. Lett.* **2006**, *8*, 4621-4.
40. Tran, N. T.; Wilson, S. O.; Franz, A. K., Cooperative hydrogen-bonding effects in silanediol catalysis. *Org. Lett.* **2012**, *14*, 186-9.
41. Beemelmans, C.; Husmann, R.; Whelligan, D. K.; Özçubukçu, S.; Bolm, C., Planar-Chiral Bis-silanols and Diols as H-Bonding Asymmetric Organocatalysts. *Eur. J. Org. Chem.* **2012**, *2012*, 3373-3376.
42. Wieting, J. M.; Fisher, T. J.; Schafer, A. G.; Visco, M. D.; Gallucci, J. C.; Mattson, A. E., Preparation and Catalytic Activity of BINOL-Derived Silanediols. *Eur. J. Org. Chem.* **2015**, (3), 525-533.
43. Kummer, V. D.; Koster, H., Contributions to the Chemistry of Halosilane Adducts. *Zeitschrift für Anorganische und allgemeine chemie* **1973**, *398*, 279-292.
44. Maguylo, C.; Chukwu, C.; Aun, M.; Monroe, B.; Ceccarelli, C.; Jones, D. S.; Merkert, J. W.; Donovan-Merkert, B. T.; Schmedake, T. A., Exploring the structure and redox activity of hexacoordinate bis(bipyridyl)silicon(IV) complexes. *Polyhedron* **2015**, *94*, 52-58.
45. Liu, H. L.; Ohmori, Y.; Kojima, M.; Yoshikawa, Y., Stereochemistry of six-coordinate octahedral silicon(IV) complexes containing 2,2'-bipyridine. *Journal of Coordination Chemistry* **1997**, *44* (3), 257-268.
46. Ricci, A.; Herrera, R. P.; Dessole, G., H-Bonding Organocatalysed Friedel-Crafts Alkylation of Aromatic and Heteroaromatic Systems with Nitroolefins. *Synlett* **2004**, 2374-2378.
47. Jeganathan, M.; Kanagaraj, K.; Dhakshinamoorthy, A.; Pitchumani, K., Michael addition of indoles to β -nitrostyrenes catalyzed by HY zeolite under solvent-free conditions. *Tetrahedron Letters* **2014**, *55*, 2061-2064.
48. Lin, C.; Hsu, J.; Sastry, M. N. V.; Fang, H.; Tu, Z.; Liu, J.-T.; Ching-Fa, Y., I₂-catalyzed Michael addition of indole and pyrrole to nitroolefins. *Tetrahedron* **2005**, *61*, 11751-11757.
49. Shokri, A.; Wang, X. B.; Kass, S. R., Electron-withdrawing trifluoromethyl groups in combination with hydrogen bonds in polyols: Bronsted acids, hydrogen-bond catalysts, and anion receptors. *J. Am. Chem. Soc.* **2013**, *135*, 9525-30.

50. Shokri, A.; Wang, X. B.; Wang, Y.; O'Doherty, G. A.; Kass, S. R., Flexible Acyclic Polyol-Chloride Anion Complexes and Their Characterization by Photoelectron Spectroscopy and Variable Temperature Binding Constant Determinations. *J. Phys. Chem. A* **2016**, *120*, 1661-8.
51. Beletskiy, E. V.; Schmidt, J.; Wang, X. B.; Kass, S. R., Three hydrogen bond donor catalysts: oxyanion hole mimics and transition state analogues. *J. Am. Chem. Soc.* **2012**, *134*, 18534-7.
52. Murugavel, R.; Voigt, A.; Walawalkar, M. G.; Roesky, H. W., Hetero- and Metallasiloxanes Derived from Silanediols, Disilanol, Silanetriols, and Trisilanol. *Chem. Rev.* **1996**, *96*, 2205-2236.
53. Muragavel, R.; Chandrasekhar, V.; Voigt, A.; Roesky, H. W.; Schmidt, H.; Noltemeyer, M., New Lipophilic Air-Stable Silanetriols: First Example of an X-ray Crystal Structure of a Silanetriol with Si-N Bonds. *Organometallics* **1995**, *14*, 5298-5301.
54. Roca-Lopez, D.; Marques-Lopez, E.; Alcaine, A.; Merino, P.; Herrera, R. P., A Friedel-Crafts alkylation mechanism using an aminoindanol-derived thiourea catalyst. *Org. Biomol. Chem.* **2014**, *12*, 4503-10.
55. Inokuma, T.; Furukawa, M.; Uno, T.; Suzuki, Y.; Yoshida, K.; Yano, Y.; Matsuzaki, K.; Takemoto, Y., Bifunctional hydrogen-bond donors that bear a quinazoline or benzothiadiazine skeleton for asymmetric organocatalysis. *Chem. Eur. J.* **2011**, *17*, 10470-7.
56. Deng, F.; Liu, H.-Y., Novel Bifunctional Organocatalyst Using Sulfamide as Hydrogen Bonding Donor: Application in Asymmetric Michael Addition of Cyclic Ketones to Nitroolefins. *Syn. Comm.* **2012**, *42*, 767-774.

APPENDIX A: NMR AND IR FIGURES FOR THE SYNTHESIZED SILICON DIOLS

FIGURE 39: Infrared spectroscopy of $[\text{Si}(\text{Me}_2\text{bpy})_2(\text{OH})_2](\text{PF}_6)_2$

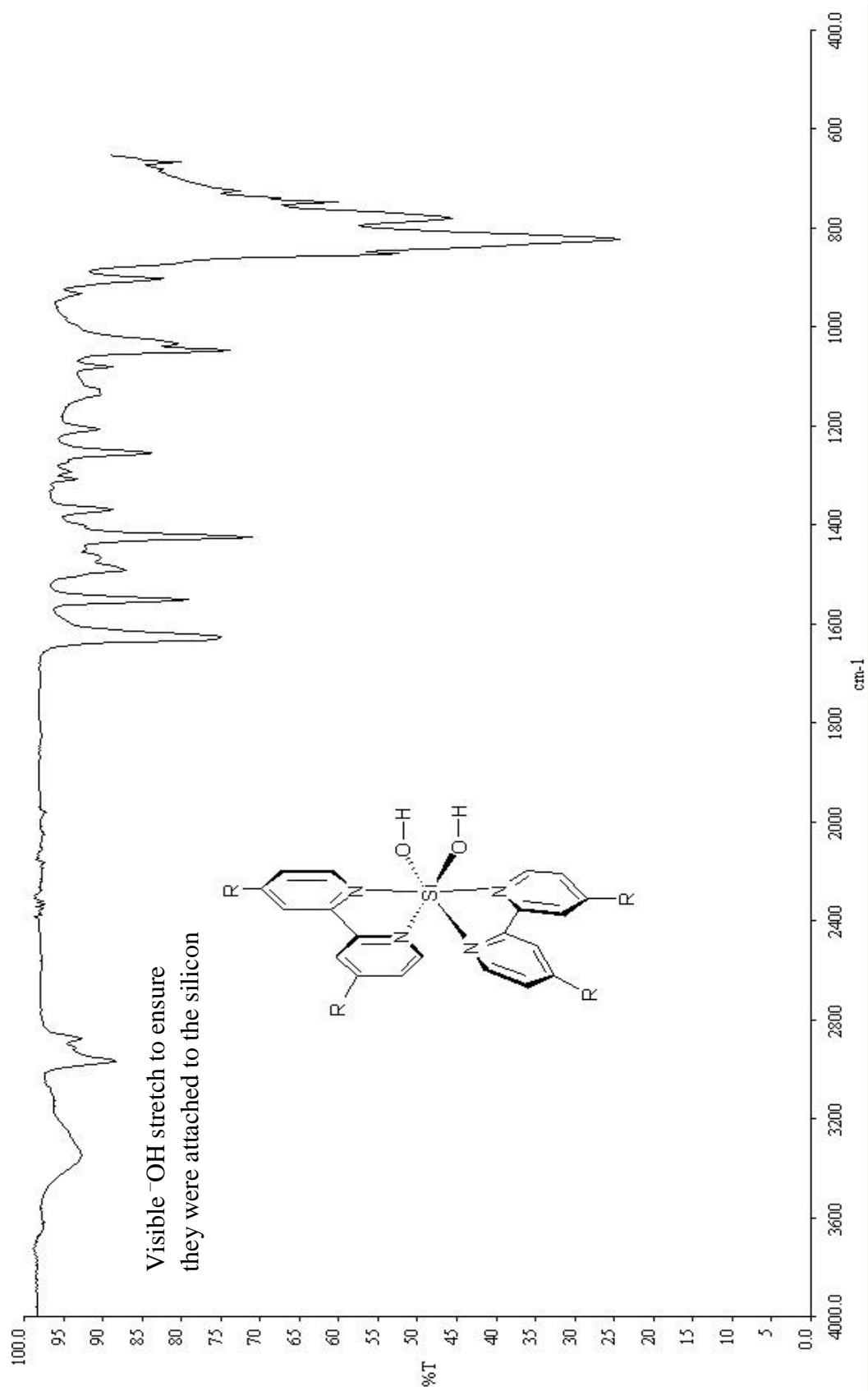




Here, the ⁻OH peak is visible
in the ¹H NMR at 3.84ppm.

FIGURE 41: ¹H NMR of [Si(Me₂bpy)₂(OH)₂](PF₆)₂

X : parts per Million : 1H

FIGURE 42: IR spectroscopy data for $[\text{Si}(\text{}^1\text{Bu}_2\text{bpy})_2(\text{OH})_2](\text{PF}_6)_2$

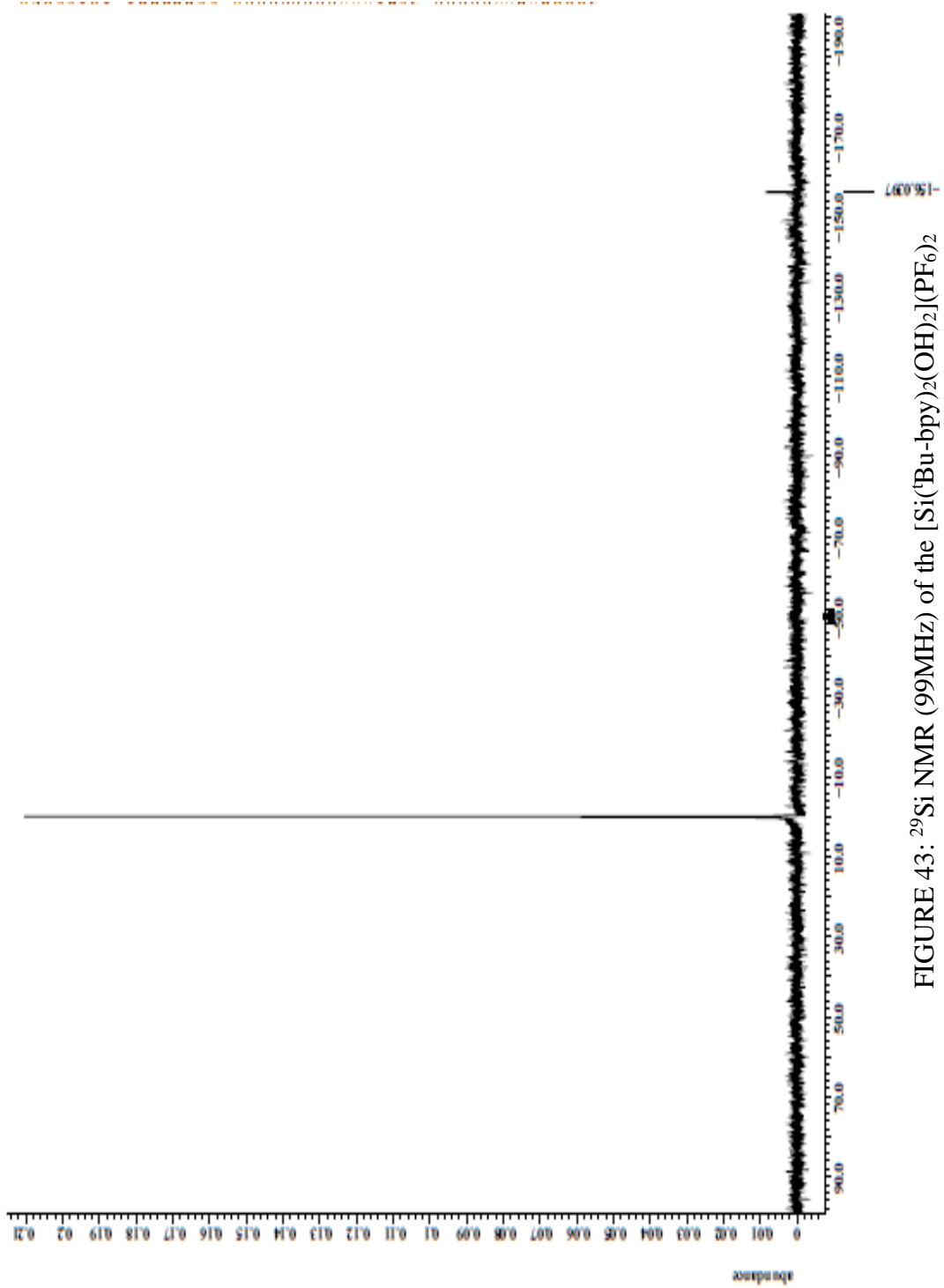
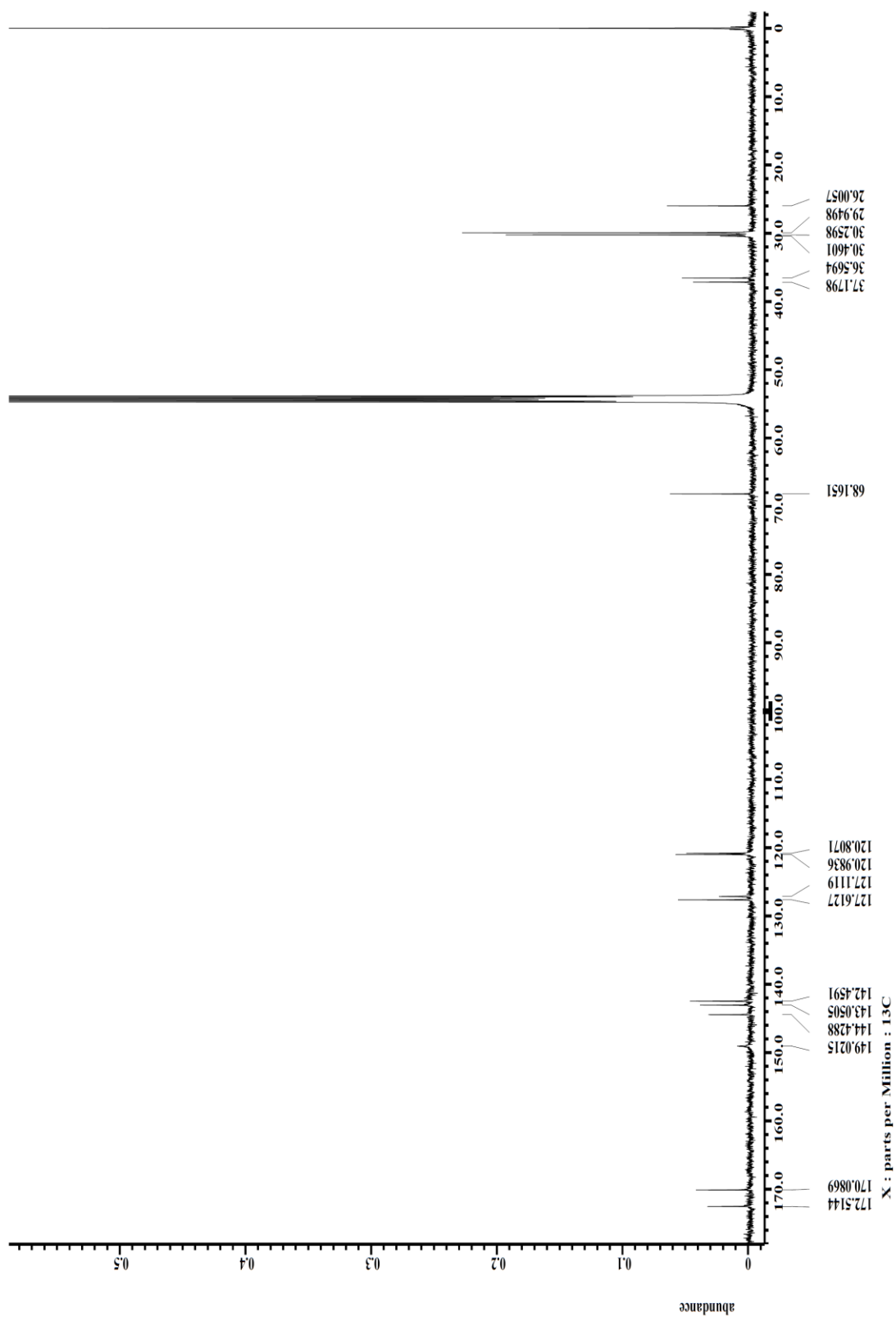


FIGURE 43: ^{29}Si NMR (99MHz) of the $[\text{Si}(\text{tBu-bpy})_2(\text{OH})_2](\text{PF}_6)_2$

FIGURE 44: ^{13}C NMR (125MHz) of $[\text{Si}(\text{tBu-bpy})_2(\text{OH})_2](\text{PF}_6)_2$ in DCM

APPENDIX B: X-RAY ANALYSIS DATA OF [Si(^tBu₂bpy)₂(OH)₂](PF₆)₂

The average length of a hydrogen bond is 1.97 Å. Hydrogen and oxygen have a van der Waals radius of 1.20 and 1.52 Å, respectively.

TABLE 1: Crystal data and structure refinement

Identification code	NS_ASOOL_X1_MO1
Empirical formula	C ₄₄ H ₅₇ N ₅ O ₄ F ₁₂ SiP ₂
Formula weight	1037.98
Temperature/K	100.05(10)
Crystal system	monoclinic
Space group	P2 ₁ /c
a/Å	14.4289(5)
b/Å	25.1380(6)
c/Å	13.2045(5)
α/°	90.00
β/°	106.293(4)
γ/°	90.00
Volume/Å ³	4597.1(3)
Z	4
ρ _{calc} /mg/mm ³	1.500
m/mm ⁻¹	0.219
F(000)	2160.0
Crystal size/mm ³	? × ? × ?
Radiation	(λ = 0.71073)
2θ range for data collection	6.7 to 57.42°
Index ranges	-19 ≤ h ≤ 19, -33 ≤ k ≤ 33, -17 ≤ l ≤ 17
Reflections collected	52129
Independent reflections	10632 [R _{int} = 0.0401, R _{sigma} = 0.0318]
Data/restraints/parameters	10632/0/573
Goodness-of-fit on F ²	1.305
Final R indexes [I ≥ 2σ (I)]	R ₁ = 0.0832, wR ₂ = 0.2878
Final R indexes [all data]	R ₁ = 0.1035, wR ₂ = 0.3135
Largest diff. peak/hole / e Å ⁻³	1.41/-0.76

TABLE 2: Bond lengths

Atom Atom	Length/Å	Atom Atom	Length/Å
P2AA O1	1.674(2)	C31 C42	1.521(4)
P2AA O2	1.651(2)	C18 C25	1.382(5)
P2AAN4	2.000(2)	C9 C17	1.381(4)
P2AAN5	1.915(3)	C27 C23	1.393(4)
P2AAN6	1.971(2)	C12 C20	1.389(4)
P2AAN7	1.915(2)	C12 C11	1.477(4)
P1 F2	1.584(3)	C28 C32	1.533(4)
P1 F8	1.612(3)	C28 C33	1.525(5)
P1 F9	1.607(3)	C28 C34	1.511(5)
P1 F10	1.568(3)	C26 C20	1.385(5)
P1 F11	1.602(3)	C26 C21	1.381(5)
P1 F12	1.566(3)	C26 C30	1.530(4)
N4 C8	1.352(4)	C13 C21	1.378(4)
N4 C9	1.333(4)	C19 C11	1.390(4)
N5 C10	1.337(4)	C19 C25	1.371(5)
N5 C11	1.337(4)	C25 C29	1.540(4)
N6 C12	1.338(4)	C37 C30	1.533(5)
N6 C13	1.357(4)	C30 C38	1.564(6)
N7 C14	1.349(4)	C30 C39	1.507(6)
N7 C15	1.349(3)	C29 C35	1.512(7)
C8 C14	1.474(4)	C29 C36	1.523(7)
C8 C16	1.375(4)	C29 C43	1.485(9)
C24 C17	1.371(4)	P2 F1	1.586(2)
C24 C28	1.529(4)	P2 F3	1.607(3)
C24 C16	1.405(4)	P2 F4	1.584(3)
C14 C22	1.376(4)	P2 F5	1.586(3)
C22 C27	1.398(4)	P2 F6	1.589(3)
C15 C23	1.363(4)	P2 F7	1.546(3)
C10 C18	1.373(4)	O3 C2	1.433(4)
C31 C27	1.526(4)	O3 C3	1.430(5)
C31 C40	1.535(5)	C2 C4	1.512(7)
C31 C41	1.523(4)	C3 C5	1.500(6)

TABLE 3: Bond Angles

Atom	Atom	Atom	Angle/°	Atom	Atom	Atom	Angle/°
O1	P2AA	N4	90.92(10)	C10	C18	C25	120.0(3)
O1	P2AA	N5	93.63(11)	N4	C9	C17	122.6(3)
O1	P2AA	N6	171.43(10)	C22	C27	C31	120.1(3)
O1	P2AA	N7	94.66(10)	C23	C27	C22	116.9(3)
O2	P2AA	O1	99.23(10)	C23	C27	C31	123.0(3)
O2	P2AA	N4	168.90(11)	C15	C23	C27	120.7(3)
O2	P2AA	N5	94.87(10)	C24	C17	C9	120.4(3)
O2	P2AA	N6	87.99(10)	N6	C12	C20	122.7(3)
O2	P2AA	N7	94.60(10)	N6	C12	C11	113.2(2)
N5	P2AA	N4	88.91(10)	C20	C12	C11	123.9(3)
N5	P2AA	N6	81.08(10)	C24	C28	C32	111.1(3)
N5	P2AA	N7	166.26(11)	C33	C28	C24	108.7(3)
N6	P2AA	N4	82.28(10)	C33	C28	C32	108.7(3)
N7	P2AA	N4	80.01(10)	C34	C28	C24	108.6(3)
N7	P2AA	N6	89.33(10)	C34	C28	C32	109.4(3)
F2	P1	F8	89.73(14)	C34	C28	C33	110.3(3)
F2	P1	F9	88.53(13)	C20	C26	C30	122.4(3)
F2	P1	F11	176.89(18)	C21	C26	C20	117.4(3)
F9	P1	F8	88.08(17)	C21	C26	C30	120.1(3)
F10	P1	F2	91.80(15)	C8	C16	C24	119.8(3)
F10	P1	F8	88.11(16)	N6	C13	C21	121.7(3)
F10	P1	F9	176.17(18)	C12	C20	C26	119.6(3)
F10	P1	F11	90.33(16)	C25	C19	C11	119.5(3)
F11	P1	F8	88.06(17)	C13	C21	C26	120.7(3)
F11	P1	F9	89.21(14)	N5	C11	C12	112.9(3)
F12	P1	F2	90.94(17)	N5	C11	C19	121.6(3)
F12	P1	F8	176.91(18)	C19	C11	C12	125.4(3)
F12	P1	F9	88.92(18)	C18	C25	C29	121.1(3)
F12	P1	F10	94.89(18)	C19	C25	C18	118.1(3)
F12	P1	F11	91.15(19)	C19	C25	C29	120.8(3)
C8	N4	P2AA	115.57(18)	C26	C30	C37	107.3(3)
C9	N4	P2AA	126.4(2)	C26	C30	C38	111.2(3)
C9	N4	C8	118.0(2)	C37	C30	C38	107.2(3)
C10	N5	P2AA	123.7(2)	C39	C30	C26	109.8(3)
C11	N5	P2AA	117.3(2)	C39	C30	C37	110.4(4)
C11	N5	C10	119.1(3)	C39	C30	C38	110.9(4)
C12	N6	P2AA	115.22(19)	C35	C29	C25	111.7(3)
C12	N6	C13	117.8(3)	C35	C29	C36	107.9(4)
C13	N6	P2AA	127.0(2)	C36	C29	C25	106.8(3)

(Table 3 continued)

C14	N7	P2AA	118.88(19)	C43	C29	C25	110.8(4)
C15	N7	P2AA	122.3(2)	C43	C29	C35	112.5(7)
C15	N7	C14	118.8(2)	C43	C29	C36	106.7(7)
N4	C8	C14	112.9(2)	F1	P2	F3	87.98(15)
N4	C8	C16	122.1(3)	F4	P2	F1	90.71(17)
C16	C8	C14	125.0(2)	F4	P2	F3	86.70(17)
C17	C24	C28	123.2(2)	F4	P2	F5	89.28(19)
C17	C24	C16	117.0(3)	F4	P2	F6	175.2(2)
C16	C24	C28	119.7(3)	F5	P2	F1	176.5(2)
N7	C14	C8	112.5(2)	F5	P2	F3	88.5(2)
N7	C14	C22	121.7(2)	F5	P2	F6	92.5(2)
C22	C14	C8	125.8(2)	F6	P2	F1	87.22(18)
C14	C22	C27	120.0(3)	F6	P2	F3	88.9(2)
N7	C15	C23	121.8(3)	F7	P2	F1	91.0(2)
N5	C10	C18	121.6(3)	F7	P2	F3	178.45(19)
C27	C31	C40	109.5(2)	F7	P2	F4	94.5(3)
C27	C31	C41	111.1(3)	F7	P2	F5	92.5(3)
C27	C31	C42	107.4(3)	F7	P2	F6	89.9(3)
C41	C31	C40	109.3(3)	C3	O3	C2	112.7(3)
C41	C31	C42	108.8(3)	O3	C2	C4	111.6(4)
C42	C31	C40	110.7(3)	O3	C3	C5	108.1(3)

APPENDIX C: X-RAY DATA ANALYSIS OF [Si(^tBu₂bpy)₂(OH)₂]₂I₂

TABLE 4: Crystal data and structure refinement

Identification code	knf_tas_si(bbb)2(oh)2_x4_mo1_2
Empirical formula	C ₃₆ H ₅₀ I ₂ N ₄ O ₂ Si
Formula weight	852.69
Temperature/K	293(2)
Crystal system	triclinic
Space group	P-1
a/Å	10.5300(2)
b/Å	11.7750(2)
c/Å	13.4187(3)
α/°	114.821(2)
β/°	98.240(2)
γ/°	102.228(2)
Volume/Å ³	1424.36(5)
Z	2
ρ _{calc} /mg/mm ³	1.988
m/mm ⁻¹	2.297
F(000)	860.0
Crystal size/mm ³	? × ? × ?
Radiation	(λ = 0.71073)
2θ range for data collection	6.94 to 65.38°
Index ranges	-15 ≤ h ≤ 15, -17 ≤ k ≤ 15, 0 ≤ l ≤ 20
Reflections collected	8947
Independent reflections	8947 [R _{int} = 0.0000, R _{sigma} = 0.0184]
Data/restraints/parameters	8947/0/347
Goodness-of-fit on F ²	0.856
Final R indexes [I >= 2σ (I)]	R ₁ = 0.0256, wR ₂ = 0.0981
Final R indexes [all data]	R ₁ = 0.0259, wR ₂ = 0.0990
Largest diff. peak/hole / e Å ⁻³	1.21/-1.18

TABLE 5: Bond Lengths

Atom	Atom	Length/Å	Atom Atom	Length/Å
Si4	O1	1.6725(12)	C13 C14	1.394(2)
Si4	O2	1.6718(13)	C13 C21	1.503(2)
Si4	N1	1.9886(14)	C13 C12	1.394(3)

(Table 5 continued)

Si4	N3	1.9406(15)	C1	C6	1.469(2)
Si4	N4	1.9350(14)	C4	C3	1.392(2)
Si4	N2	1.9916(13)	C4	C5	1.383(2)
N1	C10	1.344(2)	C16	C17	1.385(2)
N1	C6	1.3580(18)	C16	C15	1.469(2)
N3	C11	1.351(2)	C3	C24	1.502(2)
N3	C15	1.353(2)	C10	C9	1.375(2)
C2	C1	1.386(2)	C18	C17	1.392(2)
C2	C3	1.395(2)	C18	C22	1.499(2)
N4	C1	1.3530(19)	C18	C19	1.396(2)
N4	C5	1.345(2)	C8	C9	1.404(2)
N2	C16	1.3513(19)	C8	C23	1.493(2)
N2	C20	1.346(2)	C20	C19	1.388(2)
C7	C8	1.398(2)	C11	C12	1.383(2)
C7	C6	1.389(2)	C14	C15	1.389(2)

TABLE 6: Bond Angles

Atom	Atom	Atom	Angle/°	Atom	Atom	Atom	Angle/°
O1	Si4	N1	86.87(6)	C2	C1	C6	124.60(14)
O1	Si4	N3	93.75(6)	N4	C1	C2	122.25(14)
O1	Si4	N4	94.36(6)	N4	C1	C6	113.15(13)
O1	Si4	N2	168.54(6)	C5	C4	C3	120.40(15)
O2	Si4	O1	103.69(7)	N2	C16	C17	122.72(15)
O2	Si4	N1	168.72(6)	N2	C16	C15	113.26(13)
O2	Si4	N3	93.44(6)	C17	C16	C15	123.99(14)
O2	Si4	N4	94.16(6)	C2	C3	C24	120.57(15)
O2	Si4	N2	86.56(6)	C4	C3	C2	117.63(14)
N1	Si4	N2	83.30(5)	C4	C3	C24	121.79(15)
N3	Si4	N1	89.72(6)	N1	C10	C9	122.70(14)
N3	Si4	N2	80.35(6)	C17	C18	C22	121.88(15)
N4	Si4	N1	80.95(6)	C17	C18	C19	117.49(14)
N4	Si4	N3	167.27(6)	C19	C18	C22	120.61(15)
N4	Si4	N2	89.92(6)	C7	C8	C9	116.90(14)
C10	N1	Si4	127.28(10)	C7	C8	C23	121.77(14)
C10	N1	C6	117.83(13)	C9	C8	C23	121.32(14)
C6	N1	Si4	114.89(10)	N2	C20	C19	121.93(15)
C11	N3	Si4	123.69(11)	N1	C6	C7	122.51(14)
C11	N3	C15	118.93(14)	N1	C6	C1	113.63(13)

(Table 6 continued)

C15	N3	Si4	117.28(11)	C7	C6	C1	123.82(13)
C1	C2	C3	119.31(14)	N3	C11	C12	121.74(15)
C1	N4	Si4	117.08(10)	C15	C14	C13	119.61(15)
C5	N4	Si4	124.01(11)	C16	C17	C18	119.49(14)
C5	N4	C1	118.75(14)	N3	C15	C16	113.24(13)
C16	N2	Si4	115.62(10)	N3	C15	C14	121.80(15)
C20	N2	Si4	126.17(10)	C14	C15	C16	124.93(14)
C20	N2	C16	118.20(13)	C10	C9	C8	120.34(14)
C6	C7	C8	119.67(14)	N4	C5	C4	121.58(15)
C14	C13	C21	120.68(16)	C20	C19	C18	120.17(15)
C12	C13	C14	117.88(15)	C11	C12	C13	120.03(16)
C12	C13	C21	121.39(16)				

TABLE 7: Fractional atomic coordinates ($\times 10^4$) and equivalent isotropic displacement parameters ($\text{\AA}^2 \times 10^3$)

Atom	<i>x</i>	<i>Y</i>	<i>z</i>	<i>U</i> (eq)
I1	1084.56(12)	-2497.71(10)	1046.63(9)	21.91(5)
I2	4008(3)	3073(3)	14485(2)	21.7(5)
Si4	2929.2(4)	-2532.8(4)	7220.3(3)	12.53(9)
O1	3117.4(12)	-3926.8(12)	6279.2(10)	16.6(2)
O2	4243.1(12)	-1367.4(12)	7325.3(10)	17.2(2)
N1	1209.1(13)	-3632.9(12)	7215.5(10)	12.2(2)
N3	3848.9(13)	-2635.5(13)	8526.6(11)	14.0(2)
C2	-546.5(16)	-3139.2(15)	4925.7(12)	13.8(3)
N4	1707.1(13)	-2372.8(13)	6098.2(11)	13.5(2)
N2	2513.3(13)	-1099.6(12)	8458.0(11)	12.7(2)
C7	-1187.2(15)	-4461.4(15)	6382.5(12)	13.8(3)
C13	5228.9(17)	-2592.5(17)	10486.2(14)	17.9(3)
C1	399.1(15)	-3089.5(14)	5787.4(12)	12.0(2)
C4	1187.9(18)	-1642.0(17)	4726.4(14)	19.0(3)
C16	3086.0(15)	-841.6(14)	9528.2(12)	12.8(3)
C3	-161.0(17)	-2376.8(16)	4393.8(12)	15.9(3)
C10	1036.0(16)	-4232.4(15)	7867.0(12)	15.4(3)
C18	2106.9(16)	887.5(15)	10349.2(14)	16.2(3)
C8	-1371.3(16)	-5062.5(15)	7076.8(12)	14.5(3)
C20	1746.7(16)	-368.2(15)	8321.9(13)	16.8(3)
C6	102.4(14)	-3772.8(14)	6464.2(12)	11.8(2)
C11	4520.3(16)	-3514.8(16)	8450.1(14)	16.6(3)
C14	4551.3(16)	-1674.9(15)	10558.3(13)	15.3(3)

(Table 7 continued)

C17	2908.1(16)	133.6(15)	10481.7(13)	14.9(3)
C15	3872.0(15)	-1721.4(15)	9568.8(13)	13.4(3)
C9	-209.5(16)	-4941.5(15)	7821.7(13)	15.8(3)
C5	2096.1(17)	-1669.9(16)	5562.7(13)	17.5(3)
C24	-1182(2)	-2339(2)	3512.4(16)	23.4(3)
C22	1839(2)	1924.6(18)	11347.6(15)	24.4(4)
C19	1523.2(17)	619.6(16)	9241.9(14)	17.8(3)
C23	-2739.1(17)	-5775.8(19)	7049.7(16)	22.7(3)
C21	5908(2)	-2611(2)	11541.6(16)	26.1(4)
C12	5209.4(17)	-3517.4(17)	9406.7(15)	19.1(3)
O3	7677.1(17)	-4732.0(18)	10136.2(15)	32.3(3)
I2A	-3916.9(9)	-12811(3)	-4541.5(12)	39.9(3)
O4	-734.6(16)	-332.8(16)	6715.8(13)	30.1(3)

TABLE 8: Anisotropic Displacement Parameters ($\text{\AA}^2 \times 10^3$)

Atom	U ₁₁	U ₂₂	U ₃₃	U ₂₃	U ₁₃	U ₁₂
I1	27.78(8)	18.87(7)	26.86(8)	13.12(5)	14.36(5)	11.95(5)
I2	10.8(5)	32.9(6)	27.9(4)	16.1(5)	9.6(3)	11.7(4)
Si4	10.89(18)	11.69(18)	11.33(17)	2.64(14)	1.11(14)	3.34(14)
O1	14.7(5)	15.4(5)	13.8(5)	1.4(4)	2.9(4)	5.2(4)
O2	13.9(5)	16.4(5)	16.5(5)	4.2(4)	3.7(4)	2.6(4)
N1	11.8(5)	10.9(5)	10.6(5)	3.0(4)	0.0(4)	3.2(4)
N3	10.7(5)	13.2(6)	15.0(5)	4.1(4)	1.6(4)	4.3(4)
C2	13.3(6)	15.1(6)	11.3(6)	4.0(5)	2.8(5)	6.2(5)
N4	12.9(6)	13.1(5)	11.1(5)	3.7(4)	1.3(4)	2.7(4)
N2	11.2(5)	11.7(5)	11.7(5)	3.1(4)	0.4(4)	3.4(4)
C7	12.8(6)	14.4(6)	11.7(6)	4.3(5)	2.0(5)	3.9(5)
C13	15.6(7)	18.8(7)	19.5(7)	10.0(6)	1.1(5)	5.6(6)
C1	11.7(6)	12.8(6)	10.2(5)	4.2(5)	2.0(5)	4.6(5)
C4	22.3(8)	20.8(7)	16.8(7)	11.4(6)	5.6(6)	6.3(6)
C16	10.5(6)	12.1(6)	13.0(6)	4.2(5)	1.2(5)	2.7(5)
C3	17.9(7)	19.2(7)	11.5(6)	6.8(5)	2.6(5)	8.7(6)
C10	15.7(7)	16.2(6)	12.6(6)	5.9(5)	0.5(5)	5.5(5)
C18	16.6(7)	12.1(6)	18.0(6)	4.1(5)	5.9(5)	5.7(5)
C8	14.9(7)	14.3(6)	12.6(6)	4.6(5)	3.7(5)	4.4(5)
C20	16.5(7)	14.8(6)	16.7(6)	4.8(5)	0.6(5)	7.9(5)
C6	11.2(6)	13.2(6)	9.2(5)	3.3(5)	1.6(4)	4.8(5)
C11	14.4(7)	14.5(6)	17.6(6)	3.9(5)	2.2(5)	7.3(5)
C14	14.5(7)	15.3(6)	13.1(6)	5.5(5)	0.4(5)	3.5(5)
C17	12.8(6)	13.9(6)	14.5(6)	4.3(5)	2.4(5)	3.1(5)
C15	11.1(6)	12.9(6)	13.3(6)	4.1(5)	0.9(5)	3.4(5)
C9	16.8(7)	15.7(6)	14.7(6)	7.8(5)	2.8(5)	3.9(5)
C5	16.7(7)	18.4(7)	16.8(6)	8.8(6)	4.1(5)	2.9(6)
C24	23.7(8)	32.1(9)	19.4(7)	15.8(7)	3.3(6)	11.5(7)
C22	28.6(9)	20.2(8)	19.5(7)	1.9(6)	7.6(6)	12.9(7)
C19	17.9(7)	15.7(7)	18.9(7)	5.9(5)	4.0(6)	8.9(6)
C23	15.4(7)	28.0(9)	24.5(8)	14.2(7)	5.2(6)	1.9(6)
C21	27.6(9)	30.8(9)	23.1(8)	15.7(7)	0.6(7)	12.4(8)
C12	15.9(7)	18.7(7)	22.3(7)	8.7(6)	2.5(6)	8.0(6)
O3	28.6(8)	27.8(8)	39.6(8)	10.6(7)	10.3(6)	16.6(7)
I2A	15.96(13)	49.6(6)	32.6(2)	0.1(2)	10.48(12)	6.1(2)

APPENDIX D: KINETIC EXPERIMENT EXTRANEOUS DATA

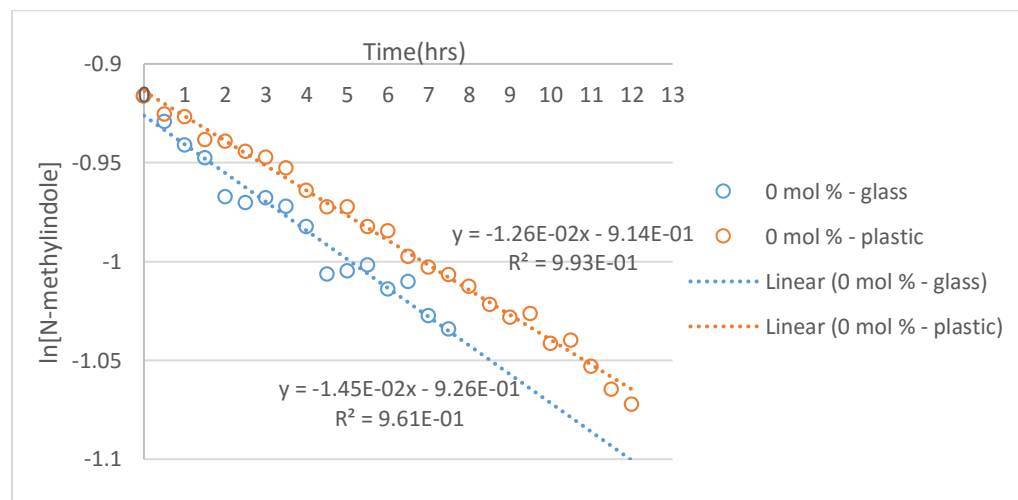


FIGURE 45: Comparison of 0 mol % catalyst loading in glass versus plastic NMR tubes in chloroform at 30 degrees Celsius

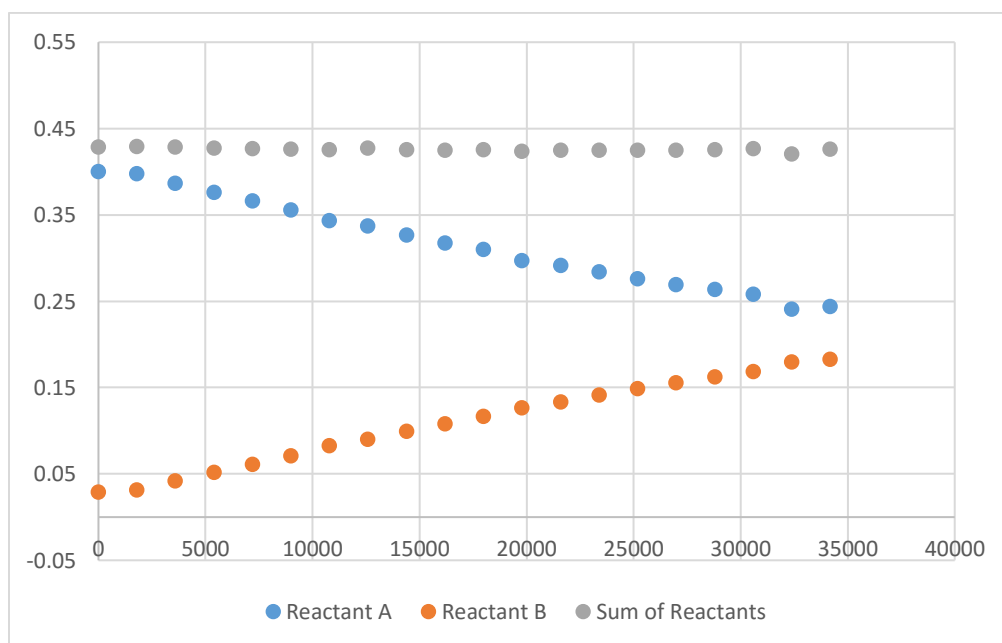


FIGURE 46: Kinetic experiment data to ensure no side products are formed

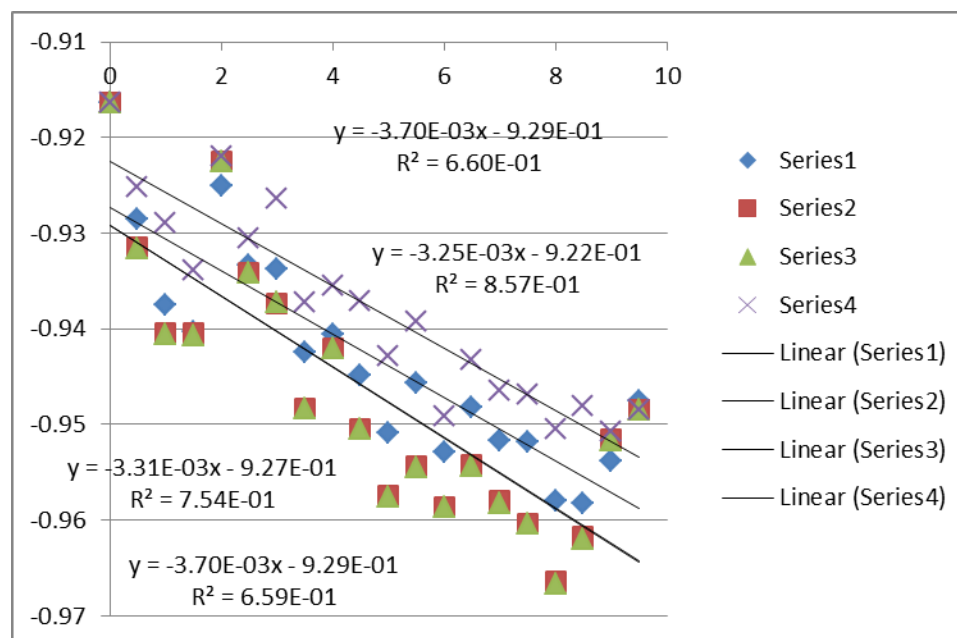


FIGURE 47: Error analysis of the 0 mol % reaction